# Electronic Supplementary Information

Controlling Selectivity for Dechlorination of Poly(Vinyl Chloride) with XantphosRhCl

Nancy Bush, [†,a] Mikiyas K. Assefa, [†,a] Selin Bac,[b] Shaama Mallikarjun Sharada[*a,b] and Megan E. Fieser[*a,c]

[a]Department of Chemistry, University of Southern California, Los Angeles, California 90089, Email: fieser@usc.edu

[b]Mork Family Department of Chemical Engineering and Materials Science, University of Southern California, Los Angeles, CA, USA, Email: ssharada@usc.edu

[c]Wrigley Institute for Environmental Studies, University of Southern California, Los Angeles, California 90089

[†]Authors contributed equally.

## 1. General Considerations

All reactions were set up under anaerobic and anhydrous conditions in a Vacuum Atmospheres OMNI glovebox under a dinitrogen atmosphere. Tetrahydrofuran (THF) was sparged with UHP argon (Praxair) and dried by passage over Q-5 and molecular sieves using a JCMeyer solvent purification system. Poly(vinyl chloride) (Aldrich, $M_n$ = 67.6 kDa, $Đ$ = 1.76 was dried under reduced pressure at 110 °C for 24 h prior to use. Commercial PVC lizard MICHLEY brand toys and CZWESTC brand bags were purchased from Amazon. For reactions, they were frozen with liquid nitrogen, ground into a powder using a coffee grinder, and dried under reduced pressure at 110 °C for 24 h prior to use. Anhydrous grade *N*,*N*-dimethylacetamide (DMA, Aldrich), $C_6D_6$ and $C_2D_2Cl_4$ (Cambridge Isotope Laboratories) were purchased from commercial suppliers and used as received.

$^1$H NMR and 13C {$^1$H} NMR spectra were recorded on a Varian 400-MR 2-Channel NMR spectrometer or a Varian VNMRS-600 3-Channel NMR spectrometer at room temperature or 110 °C and referenced against residual solvent resonances. Infrared (IR) spectra were recorded on an Agilent Cary 630 FTIR spectrometer equipped with a single reflection diamond (Di) attenuated total reflectance (ATR) module. Differential scanning calorimetry (DSC) and Thermogravimetric analysis (TGA) data were collected using a Mettler-Toledo TGA/DSC+ instrument. The thermal measurements were made at a heating rate of 10 °C/min and a dinitrogen flow rate of 40 mL/min. $T_m$ values were obtained from the peak maximum in the second heating curve, and $T_d$ was determined at 5% mass loss. Elemental analyses were carried out on a Thermo Flash 2000 Elemental Analyzer. Energy-dispersive X-ray spectroscopy (EDX) measurements were made on a Thermo Scientific Helios G4 PFIB UXe instrument equipped with an Oxford UltimMax 170 Silicon Drift Detector and processed with a Aztec software. EDX measurements were collected in

triplicate on three or four different locations of a sample (a total of 9 or 12 spectra per sample), and average values thereof are tabulated herein. Gel permeation chromatography was carried out on an Agilent 1260 Infinity II GPC instrument calibrated with monodisperse polystyrene standards at 140 °C in 1,2,4-tricholorbenzene.

Single crystal X-ray diffraction data for (xantphos)(COD)RhCl were collected on a Bruker APEX DUO 3-circle platform diffractometer equipped with an APEX II CCD detector using Cu $K_\alpha$ radiation (multi-layer mirror monochromator) from a microfocus tube. Crystals of (xantphos)(COD)RhCl were mounted on a cryoloop under Paratone-N oil, and data were collected at 100(2) K using an Oxford Cryosystems Cryostream 700 apparatus. The frames were integrated using the SAINT+ algorithm to give the hkl files corrected for Lp/decay.[1] The absorption correction was performed using the SADABS program.[2] The structures were solved by intrinsic phasing/direct methods/Patterson method and refined on F2 using the Bruker SHELXTL Software Package.[3–6] All hydrogen atom positions were idealized, and rode on the atom of attachment.

## 2. Synthesis of (xantphos)RhCl

Analogous to prior literature methods, synthesis of (xantphos)RhCl.[7–9] In a nitrogen-filled glovebox, $[Rh(COD)Cl]_2$ (COD= cyclooctadiene, 1 equiv.) and 4,5-bis(diphenylphosphino)-9,9-dimethylxanthene (xantphos, 2 equiv.) were added into a 20 mL vial that was charged with a stir bar. 10 mL of THF was subsequently added, yielding a transparent, dark red-orange solution. This mixture was stirred at room temperature for 48 h, whereupon the volatiles were removed *in vacuo*, leaving a dark orange powder. The powder was washed twice with pentanes and dried again under reduced pressure. The isolated solid was characterized by $^{1}H$ and $^{31}P$ NMR spectroscopy shown in Figures S1 and S2 below, where COD was still present. $^{1}H$ NMR (400 MHz, $C_6D_6$) δ 8.34 – 8.20 (s, 2H), 7.44 – 7.29 (s, 4H), 7.13 – 7.05 (m, 2H), 7.01 – 6.94 (m, 2H), 6.88 (dd, $J$ = 9.3, 6.0 Hz, 4H), 4.19 – 4.04 (s, 2H), **1.85 – 1.67 (s, 3H) (pentanes)**, 1.42 – 1.30 (s, 6H), 1.05 (s, 2H), **0.93 – 0.80 (m, 3H) (pentanes)**. $^{31}P$ NMR (400 MHz, $C_6D_6$) δ 0.21 – 0.49 (d, $J$ = 92.3). Crystals of (xantphos)(COD)RhCl, suitable for X-ray diffraction analysis, were grown from a hot $C_6D_6$ solution that was allowed to slowly cool to room temperature.

PVC dechlorination reactions with the above-described isolated complex were found to be comparable to that of reactions in which $[Rh(COD)Cl]_2$ and Xantphos were added directly to the reaction mixture. Therefore, all catalytic reactions were done with in situ generation of the catalyst.

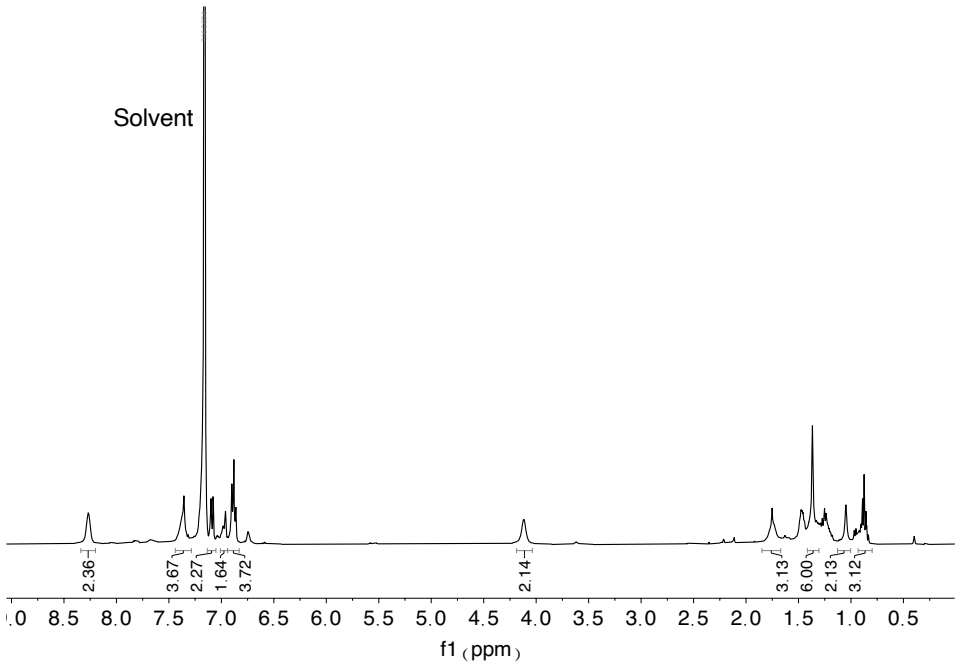


**Fig. S1** $^{1}H$ NMR spectrum of (xantphos)(COD)RhCl complex in $C_6D_6$.

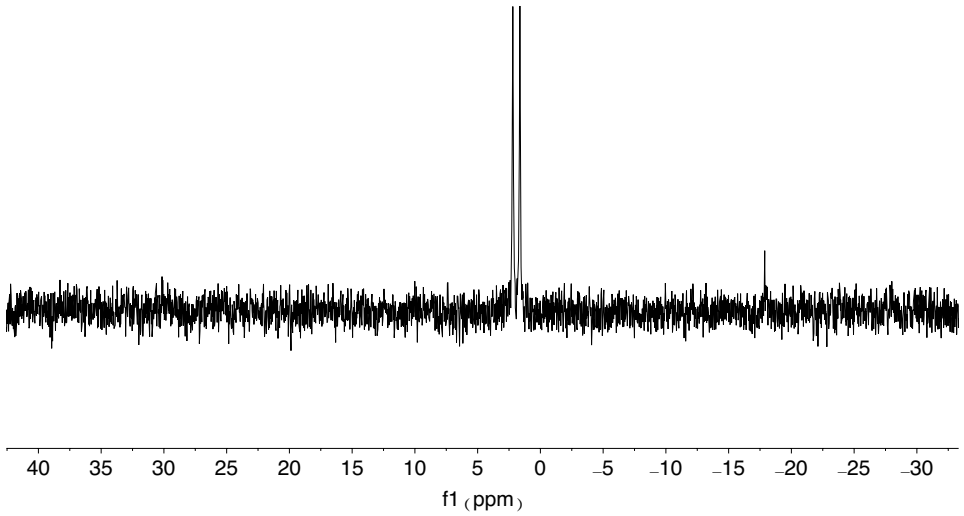


**Fig. S2** $^{31}P\{^{1}H\}$ NMR spectrum of (xantphos)(COD)RhCl complex in $C_6D_6$.

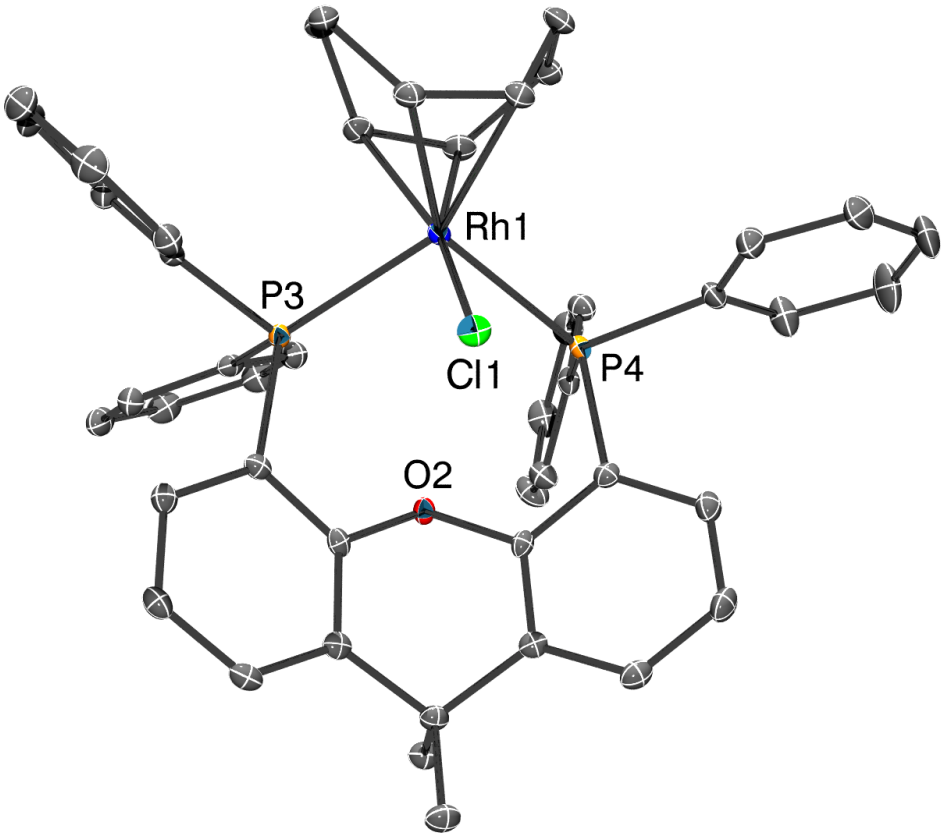


**Fig. S3** Thermal ellipsoid plot of 2[(xantphos)(COD)RhCl]·THF·$C_6D_6$, drawn at the 50% probability level. Hydrogen atoms and solvates are omitted for clarity, while only one of two molecules in the asymmetric unit shown. Selected bond distances (Å) and angles (°): Rh1-Cl1 = 2.3993(5); Rh1-P3 = 2.4054(5); Rh1-P4 = 2.5328(5); P3-Rh1-P4 = 104.644(16).

**Table S1** Crystallographic details for 2[(xantphos)(COD)RhCl]·THF·$C_6D_6$

| | **2[(xantphos)(COD)RhCl]·THF·$C_6D_6$** |
|---|---|
| Formula | $C_{104}H_{96}D_6Cl_2O_3P_4Rh_2$ |
| Crystal Habit, Color | Plate, Orange |
| Crystal Size (mm) | 0.15 × 0.15 × 0.05 |
| MW (g/mol) | 1806.49 |
| crystal system | triclinic |
| space group | P -1 |
| a (Å) | 11.4014(5) |
| b (Å) | 16.6771(7) |
| c (Å) | 22.4823(9) |
| α (°) | 99.153(2) |
| β (°) | 96.453(2) |
| γ (°) | 91.012(2) |
| V ($Å^3$) | 4190.9(3) |
| Z | 2 |
| T (K) | 100(2) |
| λ (Å) | 1.54178 |
| GOF | 1.048 |
| Density (calcd) ($Mg/m^3$) | 1.432 |
| Absorption coefficient ($mm^{-1}$) | 4.912 |
| $F_{000}$ | 1868 |
| Total no Reflections | 93826 |
| Unique Reflections | 15940 |
| Final R indices* | $R_1 = 0.0276$ |
| | $wR_2 = 0.0697$ |
| Largest Diff. peak and hole ($e^- A^{-3}$) | 0.992, -0.737 |

* For [I > 2σ(I)]

**3. General Procedures for PVC Dechlorination Reactions**

In a glovebox, $[(COD)RhCl]_2$ and xanthphos in a 1:2 molar ratio, poly(vinyl chloride) (PVC), hydride source (NaH, $NaHCO_2$ or $Et_3SiH$), and solvent (5 mL, DMA or THF) were charged into a vial equipped with a Teflon-coated cap. The vial was sealed, secured with electrical tape, brought out of the glovebox, and placed inside a preheated oil bath for the desired time. The vial was then cooled to room temperature and the mixture quenched with 5 mL of isopropanol, followed by 5 mL water, which resulted in deposition of a dark brown precipitate. The solid was allowed to settle, and the supernatant was pipette away. The isolated polymer was then dried under reduced pressure at 120 °C for 2 h.

In a few cases, the mother liquor was evaporated to dryness, and the residues were weighed and characterized by $^1H$ NMR in THF in order to identify if residual PVC was remaining. The scaled-up reaction (Table S2, entry 2c") is conducted in a 100 mL pressure flask with Teflon screw-top lid and done with all reagents and solvent at a 5x scale.

## 4. Optimization of Reaction Conditions

The tables below describe the different reaction conditions varied for this study. The characterization of the products from these reactions that were not shown in the main text are shown in the sections below.

**Table S2.** Optimizations of catalytic conditions for each hydride source.

| H Source | Entry[a] | Cat. Loading mol% (mmol) | Equiv. of H source (mmol) | Solvent[b] | Time |
|---|---|---|---|---|---|
| **$Et_3SiH$** | 1a | 1 (0.02) | 5 (10.5) | THF | 2 d |
| | 1a' | 1 (0.02) | 5 (10.5) | THF | 2 d |
| | 1b | 5 (0.08) | 5 (8.0) | THF | 2 d |
| | 1c | 1 (0.02) | 5 (10.5) | DMA | 4 d |
| | 1d | 5 (0.08) | 1 (1.6) | DMA | 2 h |
| | 1d' | 5 (0.08) | 1 (1.6) | DMA | 2 h |
| **$NaHCO_2$** | 2a | 1 (0.02) | 2 (4.2) | THF | 2 d |
| | 2b | 5 (0.08) | 2 (3.2) | THF | 1 d |
| | 2c | 5 (0.08) | 2 (3.2) | THF | 2 d |
| | 2c' | 5 (0.08) | 2 (3.2) | THF | 2 d |
| | 2c"[c] | 5 (0.08) | 2 (3.2) | THF | 2 d |
| | 2d | 5 (0.08) | 2 (3.2) | DMA | 2 d |
| | 2e | 5 (0.08) | 1 (1.6) | DMA | 2 h |
| | 2e' | 5 (0.08) | 1 (1.6) | DMA | 2 h |
| **NaH** | 3a | 1 (0.02) | 1 (2.1) | THF | 2 d |
| | 3b | 1 (0.02) | 1 (2.1) | DMA | 2 d |
| | 3c | 5 (0.08) | 1 (1.6) | THF | 2 h |
| | 3d | 5 (0.08) | 1 (1.6) | DMA | 2 h |
| | 3d' | 5 (0.08) | 1 (1.6) | DMA | 2 h |

[a]Repeat experiments are labelled with an apostrophe. [b]In all cases with 5 mol% catalyst loading, 5 mL solvent was used for 1.6 mmol PVC (102 mg). In cases with 1 mol% catalyst loading, 5 mL solvent was used for 2.1 mmol PVC (127 mg), which allowed for at least 5 mg of Rh precursor to be weighed for the reaction. Reactions were run at 110 °C. [c]This reaction was done at 5 times the scale of 2c and 2c', with all ratios the same. In this case 25 mL THF was used for 8.2 mmol PVC (510 mg).

**Table S3.** Control reactions to understand the reactivity of solvent and hydride sources.

| H Source | Entry[a] | Cat. Loading mol% (mmol) | Equiv. of H source (mmol) | Solvent |
|---|---|---|---|---|
| **None** | 1a | - | - | THF |
| | 1b | - | - | DMA |
| | 1c | 5 (0.08) | - | THF |
| | 1d | 5 (0.08) | - | DMA |
| **$Et_3SiH$** | 2a | - | 5 (10.5) | THF |
| | 2b | - | 5 (10.5) | DMA |
| **$NaHCO_2$** | 3a | - | 2 (3.2) | THF |
| | 3b | - | 2 (3.2) | DMA |
| **NaH** | 4a | - | 1 (1.6) | DMA |

[a]In cases not using $Et_3SiH$, 5 mL solvent was used for 1.6 mmol PVC (102 mg). In cases with $Et_3SiH$, 5 mL solvent was used for 2.1 mmol PVC (127 mg). All reactions were run for 2 d at 110 °C.

**5. Weights**

Unfortunately, the catalyst appears to remain in the polymer product, which prevents bulk characterization from showing quantitative evidence for exact selectivity between HDC and DHC for each H-source. We weighed the polymer product and the residues from the mother liquor. In this case, we see the recovered polymer for the sodium formate reaction is close to what is expected for PE formation. The slightly increased mass can be attributed to residual catalyst remaining in the polymer. However, NaH reactions show a similar amount of byproduct in the mother liquor (~200 mg) but a much larger mass in the polymer product. Along with residual catalyst, we hypothesize this could be due to oxidation of the alkenes generated from DHC.

**Table S4.** Following the mass recovery of reactions for evidence of side reactions.

| H Source | Entry[a] | Total Rxn Mass (g)[b] | Polymer Product Mass (g) | Mother Liquor Mass (g) | Mass % diff[b] |
|---|---|---|---|---|---|
| **$NaHCO_2$** | 2c' | 0.390 | 0.054 | 0.206 | 53 |
| **NaH** | 3d' | 0.208 | 0.126 | 0.229 | 123 |

[a]Entry from Table S2. [b]Starting PVC weight was 102 mg. [c]Polymer product weight/PVC starting weight x 100. Full conversion from PVC to PE should see a 45% mass difference.

To ensure there was no remaining PVC in the mother liquor, we evaporated the mother liquor from the $NaHCO_2$ reaction (**Table S2**, entry 2c') to dryness and characterized the residuals by ATR-IR.

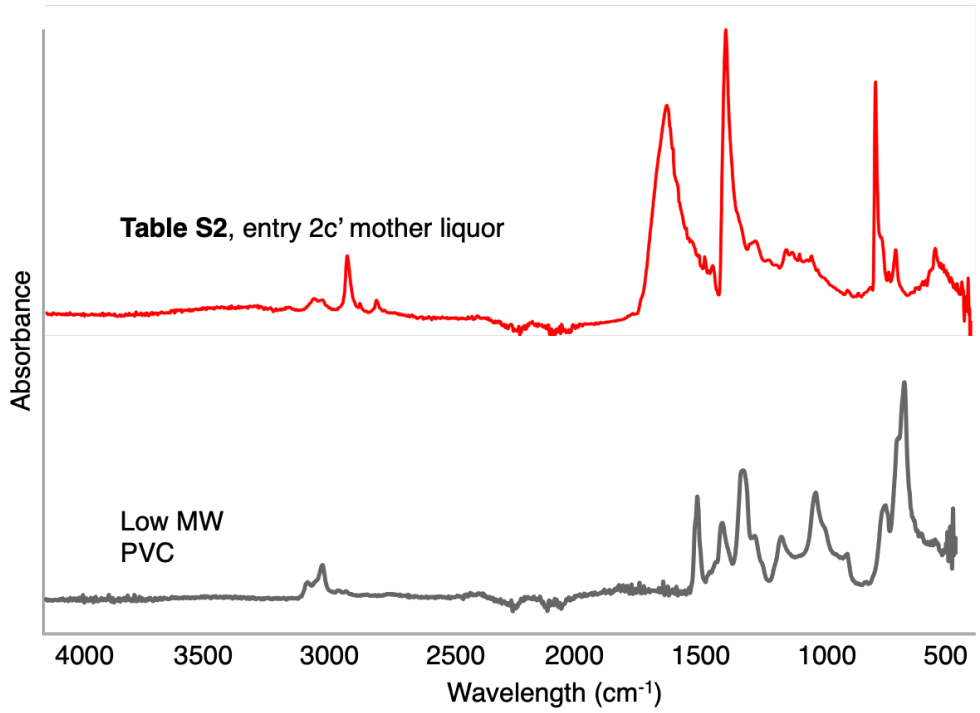


**Fig. S4** IR spectra of low molecular weight PVC (CAS: 9002-86-2, Sigma Aldrich, bottom) and solids from mother liquor of Table S2, entry 2c' (top), showing no observable PVC remaining.

The residuals were then stirred in THF at 50 °C until dissolved, and then characterized by $^{1}$H NMR spectroscopy. In addition, polymer products from Table S2, entries 2c' and 2e' were also stirred in THF at 50 °C for 2 hours and characterized by 1H NMR spectroscopy. In comparison to PVC starting material, no PVC could be identified in any of the samples (**Fig. S5**).

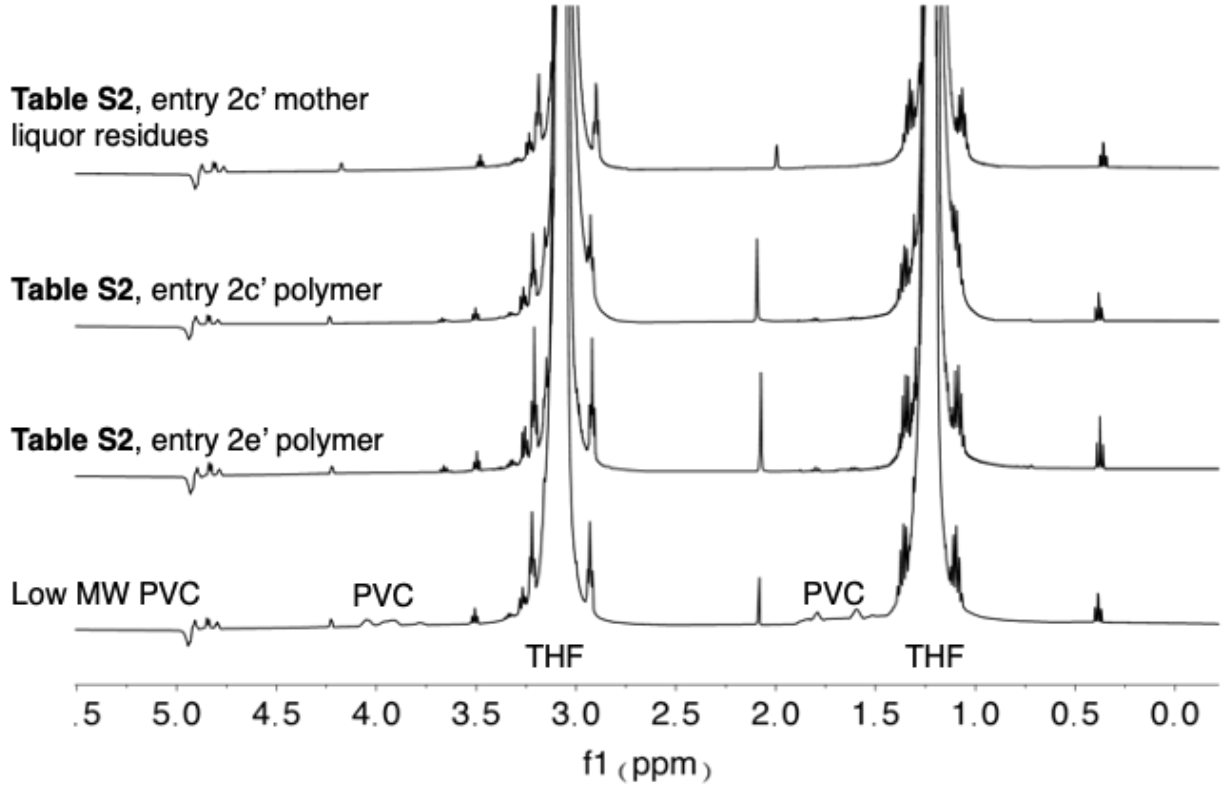


**Fig. S5** $^{1}$H NMR spectra in THF of low molecular weight PVC (CAS: 9002-86-2, Sigma Aldrich, bottom), solids from mother liquor of **Table S2**, entry 2c', and polymer products from **Table S2**, entries 2c' and 2e', showing no observable PVC remaining.

## 6. ATR-IR Spectroscopic Data

IR spectroscopy was used to identify promising reaction conditions for each H source as it is a quick and easy method to identify general characteristics of the final polymer product. The IR spectra of polyethylene and polyvinyl chloride are very different, with polyethylene showing three distinct peaks, most prominent thereof appears in the 2800-3000 $cm^{-1}$ region. The IR spectrum of poly(vinyl chloride) has a distinct C-Cl stretch between 600-650 $cm^{-1}$ that does not overlap with any polyethylene peaks, allowing us to track reaction progress by monitoring its intensity relative to those of polyethylene. While not quantitative, this method enables quick identification of conditions that yield PE-like polymers, as well as those that do not convert PVC very well. Once optimal conditions were identified, further characterization of the polymer product was carried out for holistic analysis of reaction outcomes. Repeat reactions are stacked to show the repeatability of the reaction outcomes.

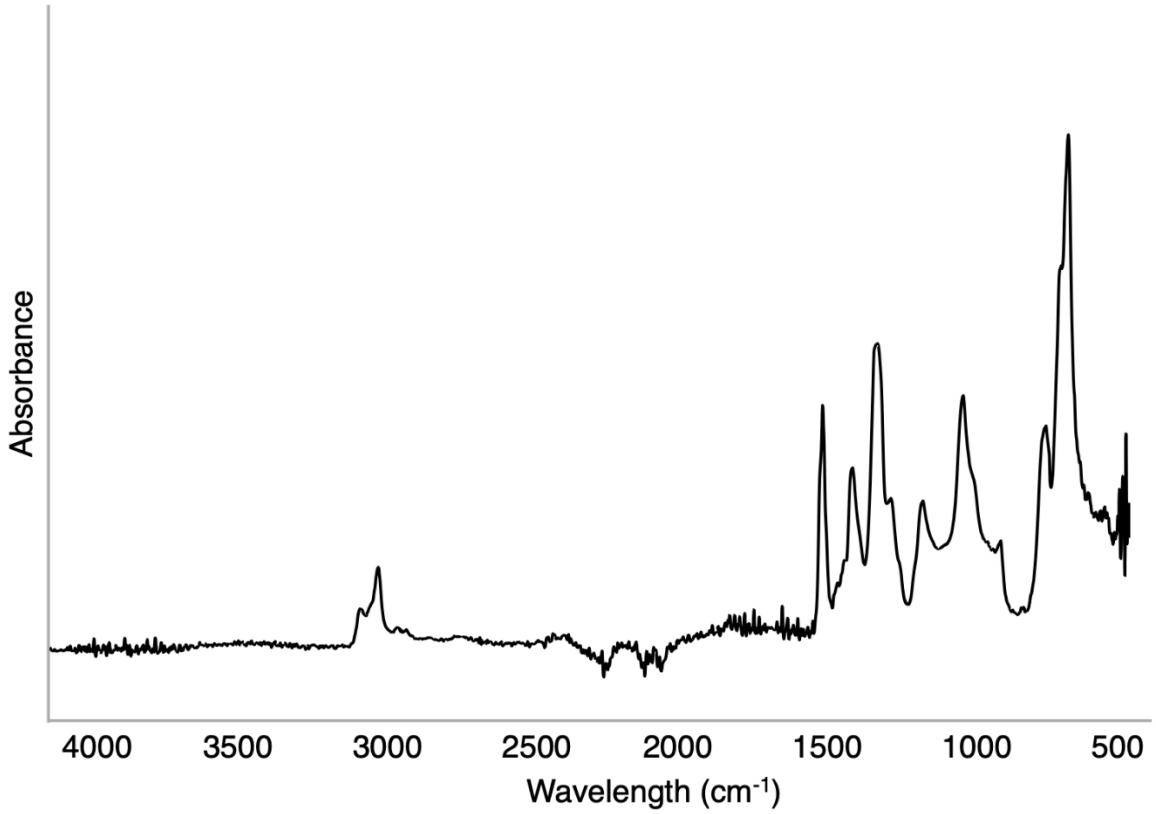


**Fig. S6** IR spectrum of low molecular weight PVC (CAS: 9002-86-2, Sigma Aldrich)

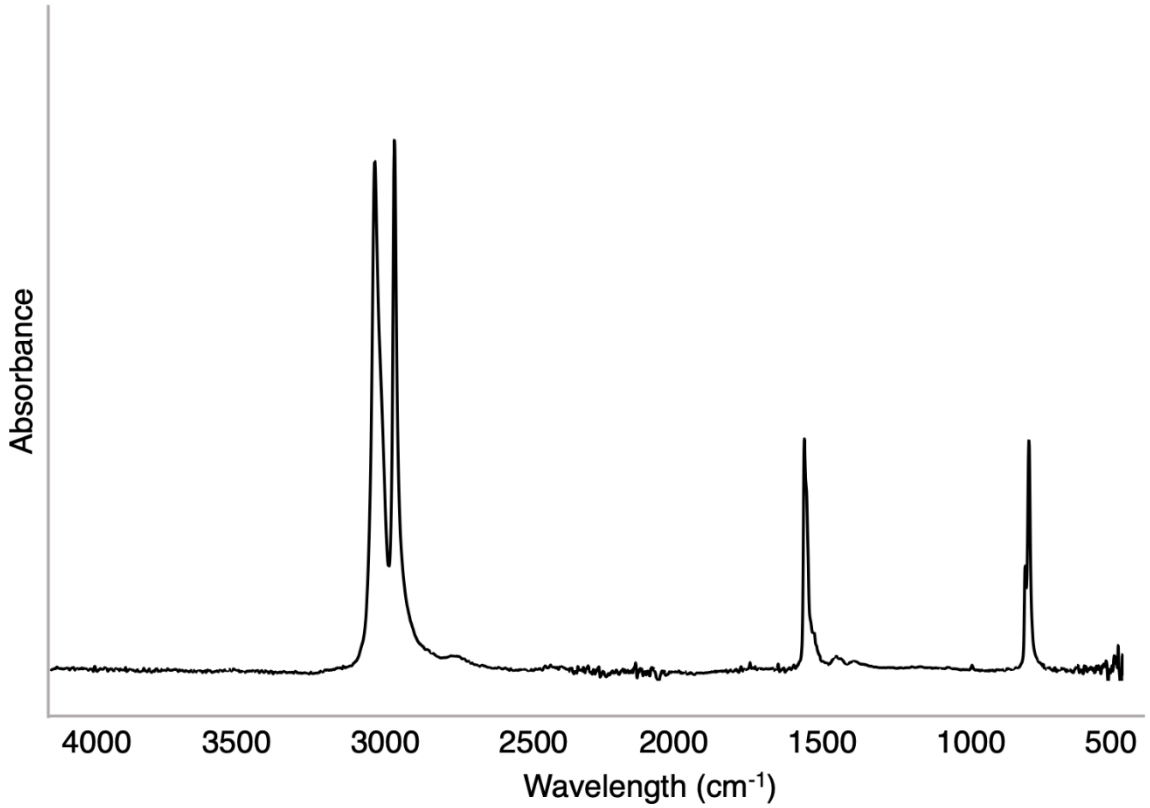


**Fig. S7** IR spectrum of HDPE pellets (CAS: 9002-88-4, Sigma Aldrich)

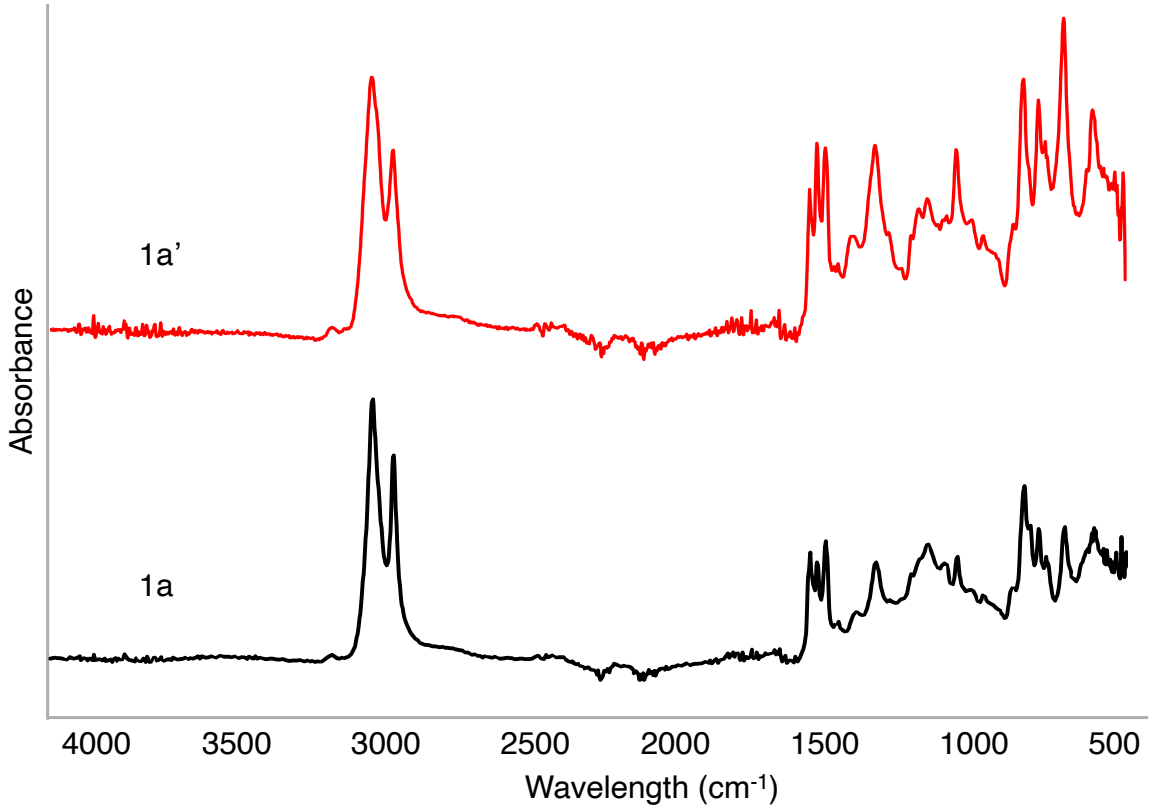


**Fig. S8** IR spectrum of Table S2, Entry 1a and Entry 1a' with the $Et_3SiH$ H source.

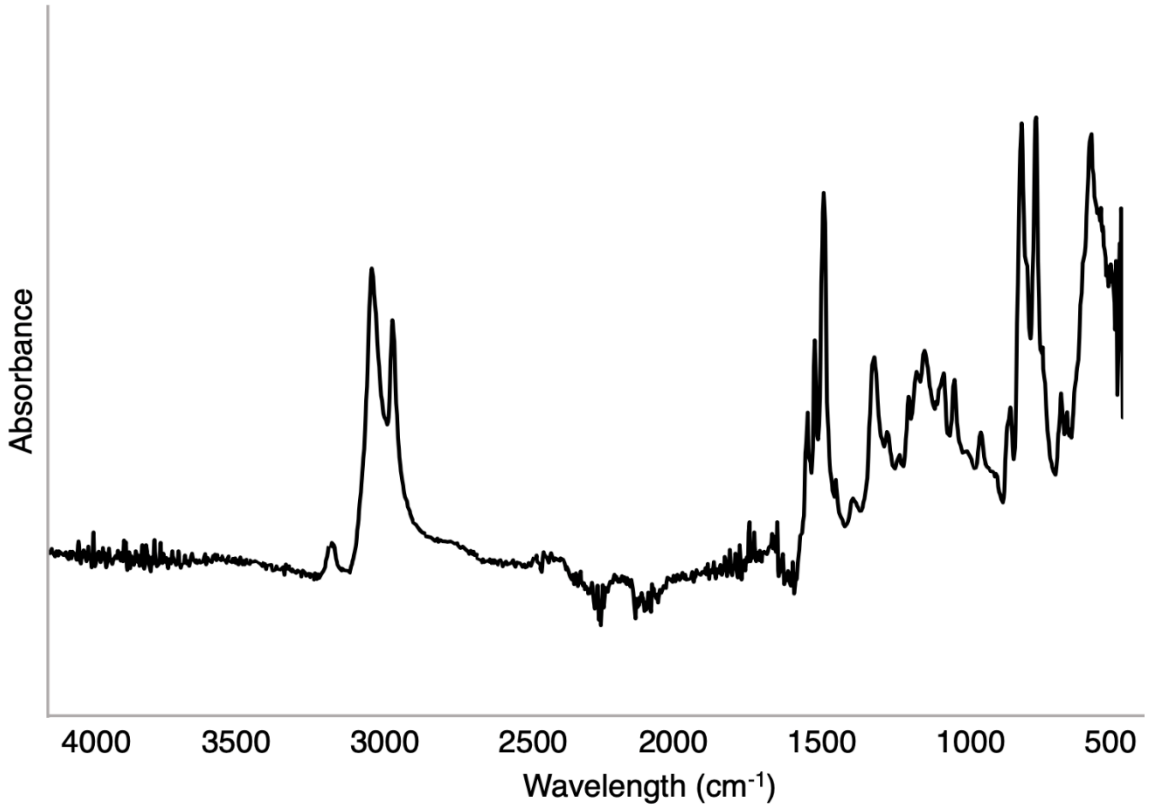


**Fig. S9** IR spectrum of Table S2, Entry 1b with the $Et_3SiH$ H source.

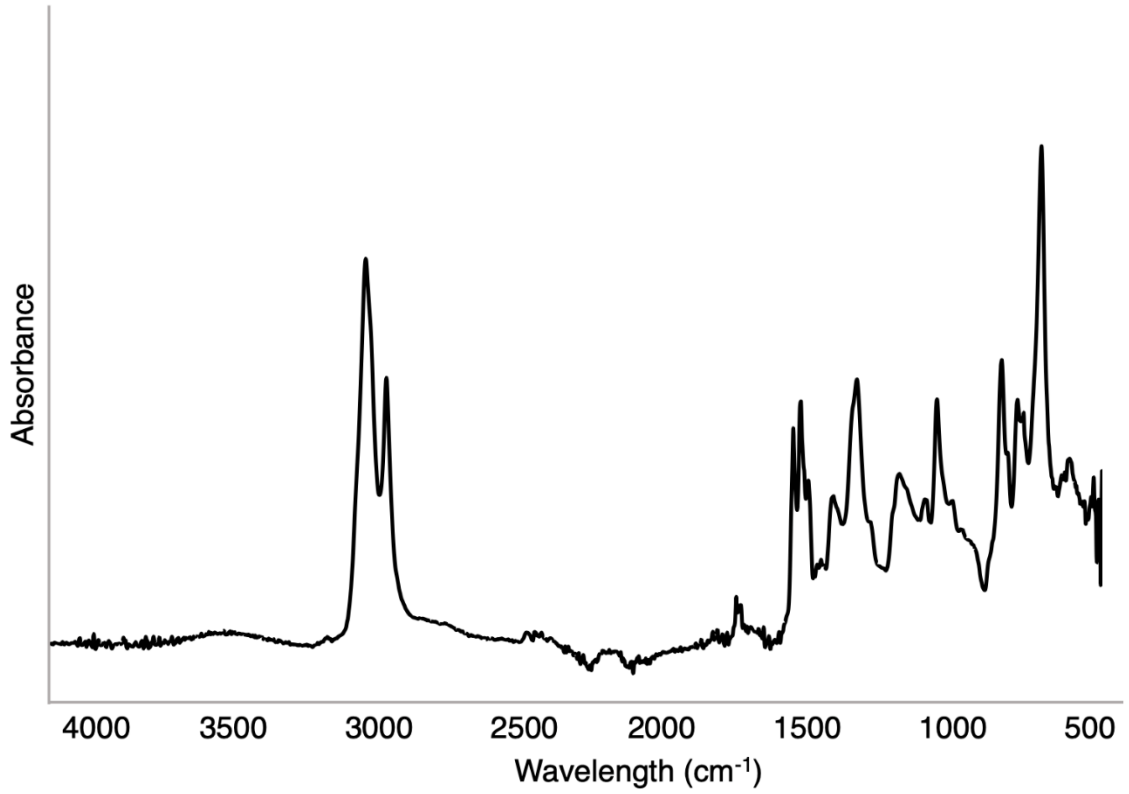


**Fig. S10** IR spectrum of Table S2, Entry 1c with the $Et_3SiH$ H source.

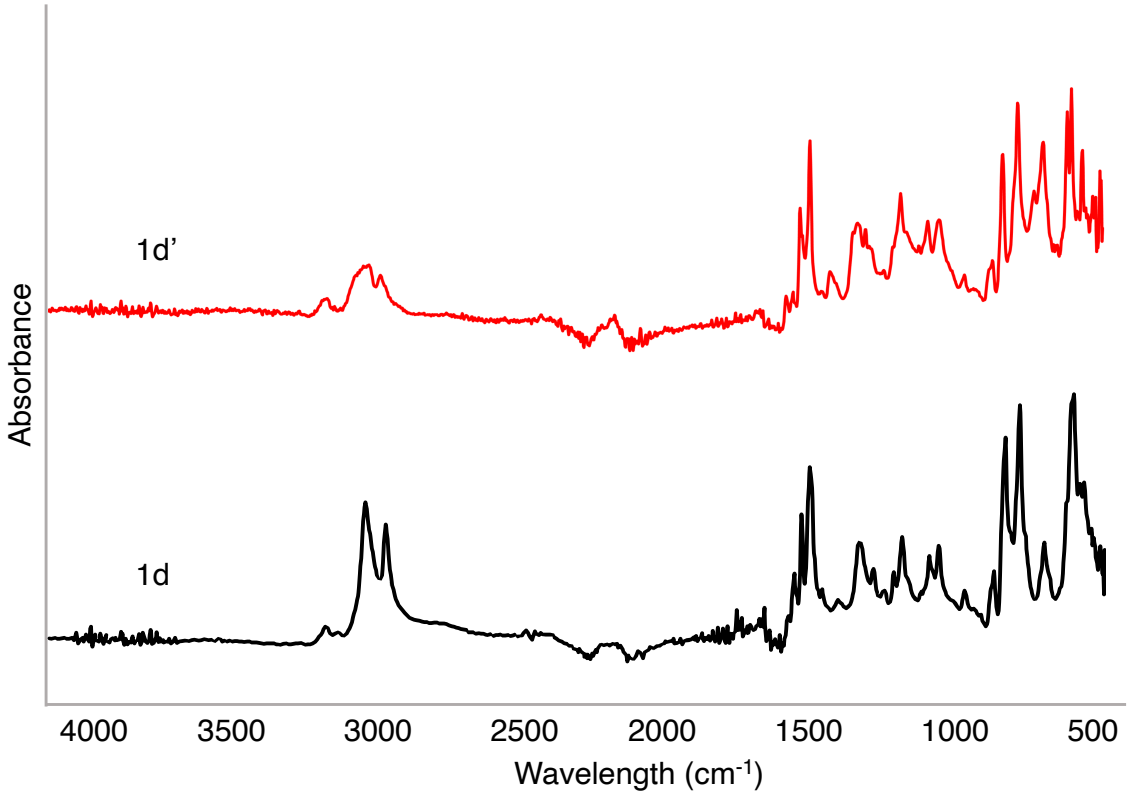


**Fig. S11** IR spectrum of Table S2, Entry 1d and Entry 1d' with the $Et_3SiH$ H source.

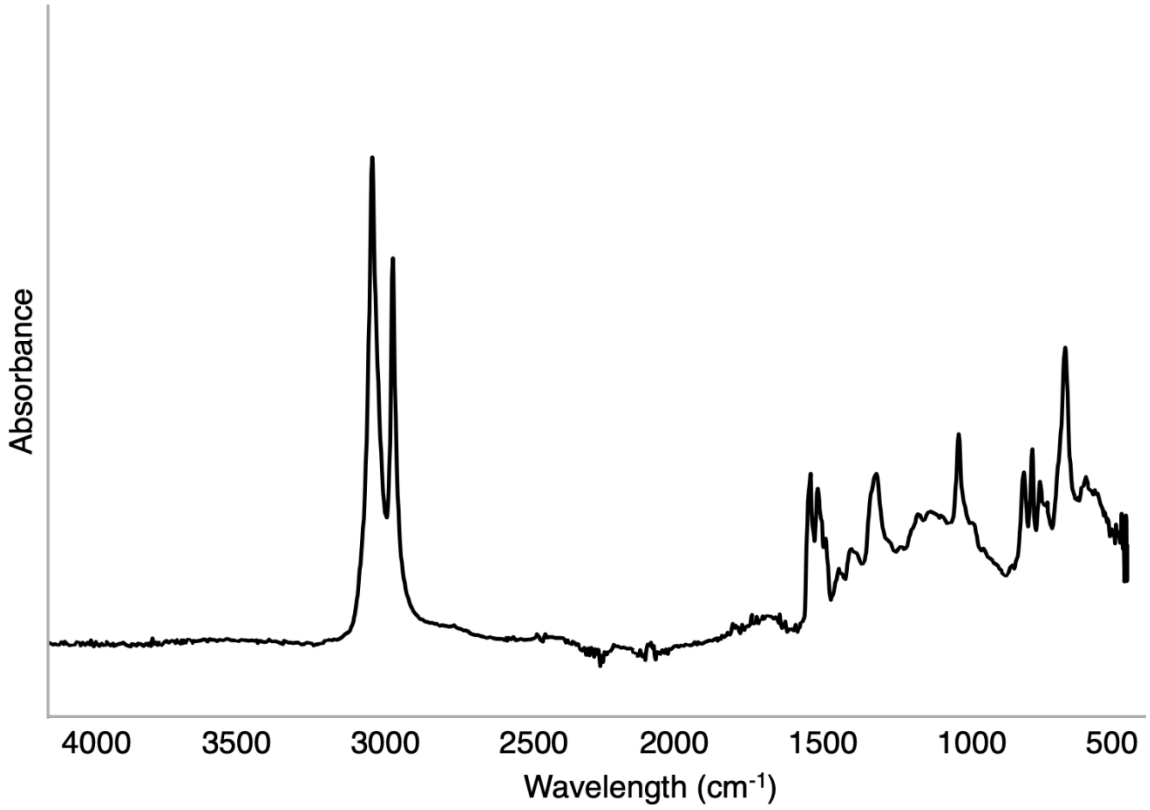


**Fig. S12** IR spectrum of Table S2, Entry 2a with the $NaHCO_2$ H source.

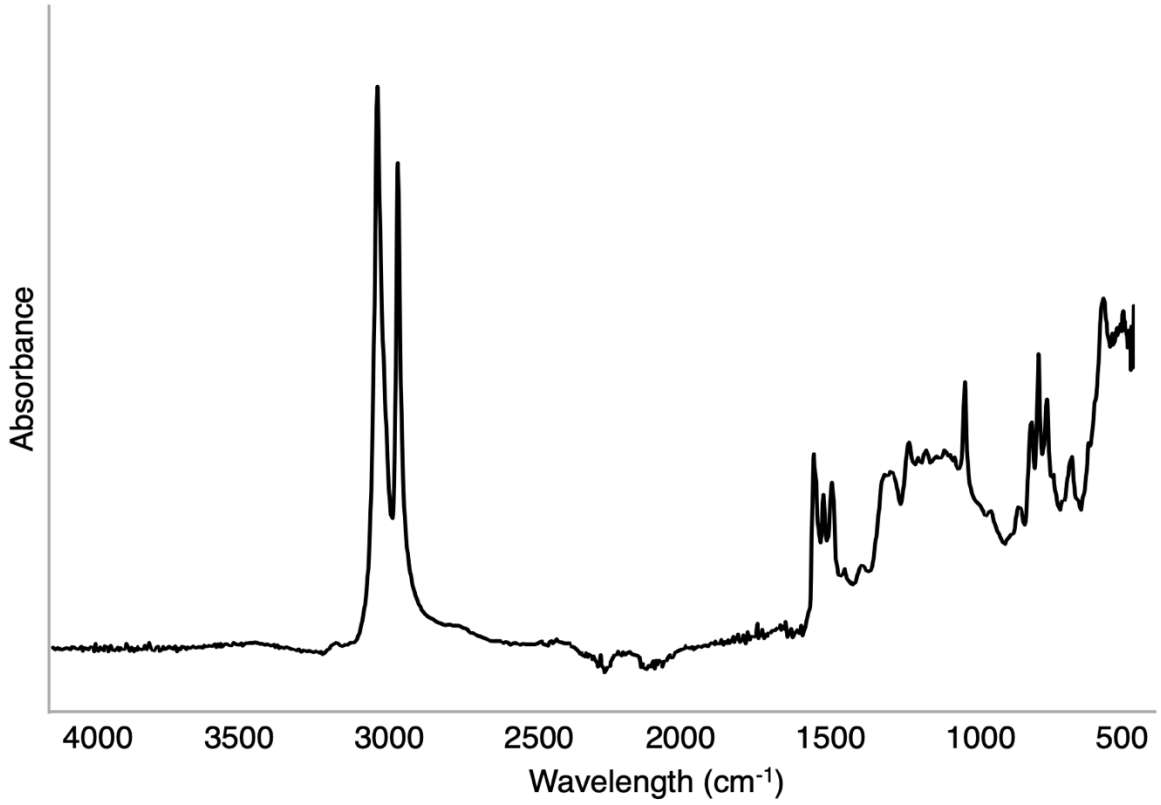


**Fig. S13** IR spectrum of Table S2, Entry 2b with the $NaHCO_2$ H source.

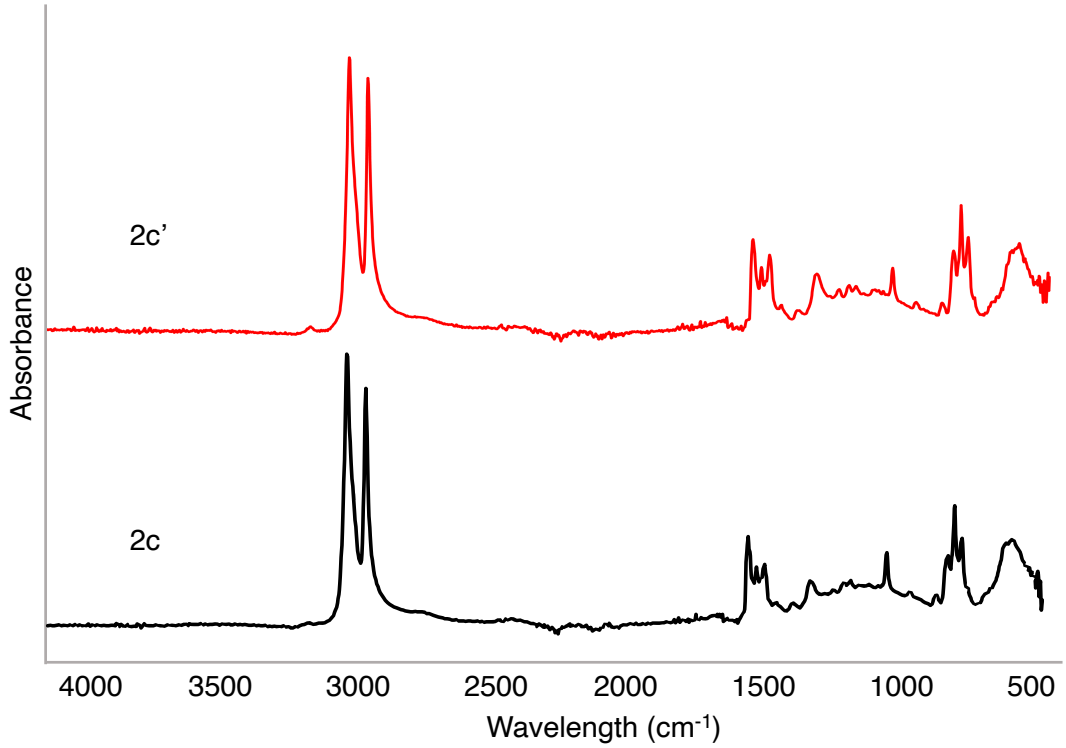


**Fig. S14** IR spectrum of Table S2, Entry 2c and 2c' with the $NaHCO_2$ H source.

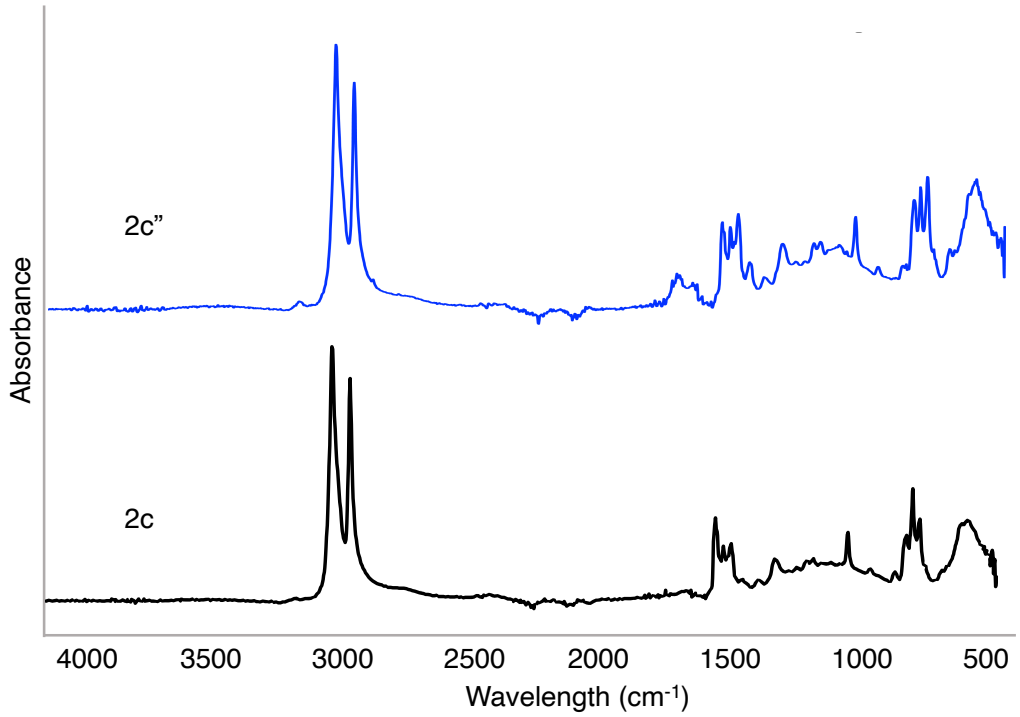


**Fig. S15** IR spectrum of Table S2, Entry 2c and 2c” with the $NaHCO_2$ H source, showing consistency of small and large scale reactions.

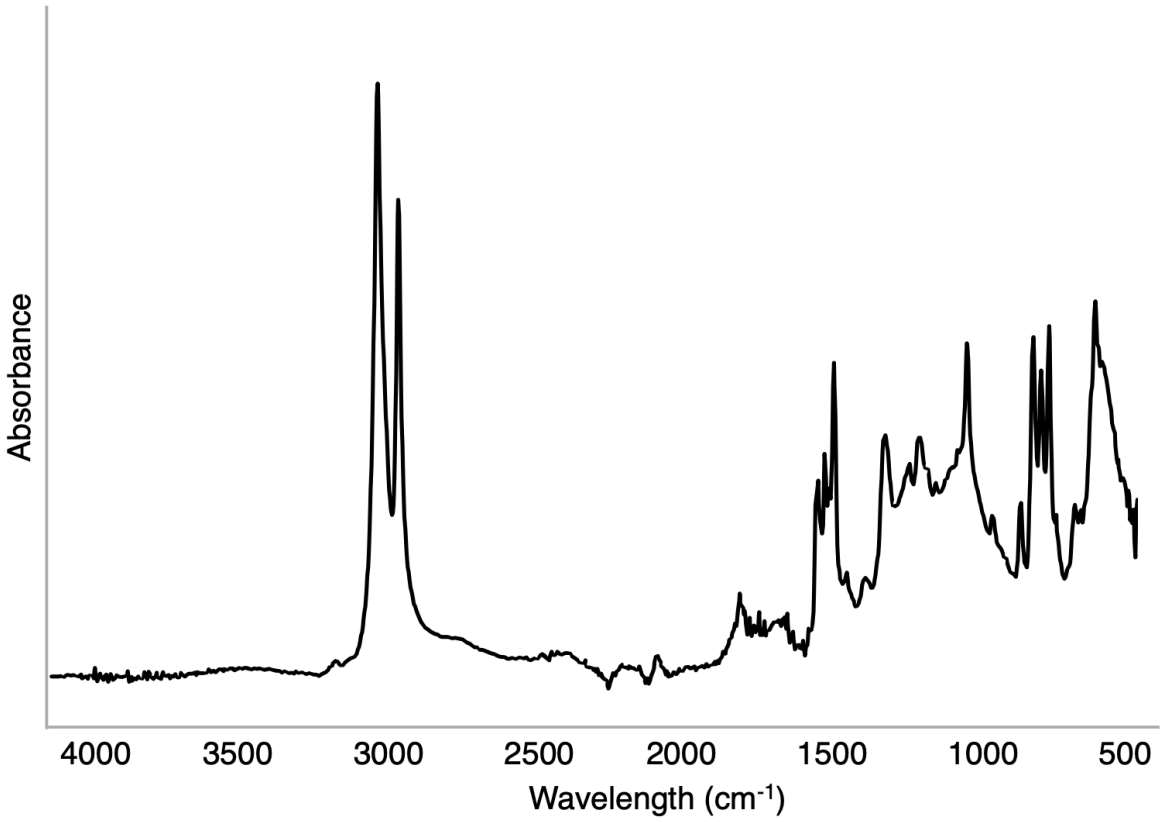


**Fig. S16** IR spectrum of Table S2, Entry 2d with the $NaHCO_2$ H source.

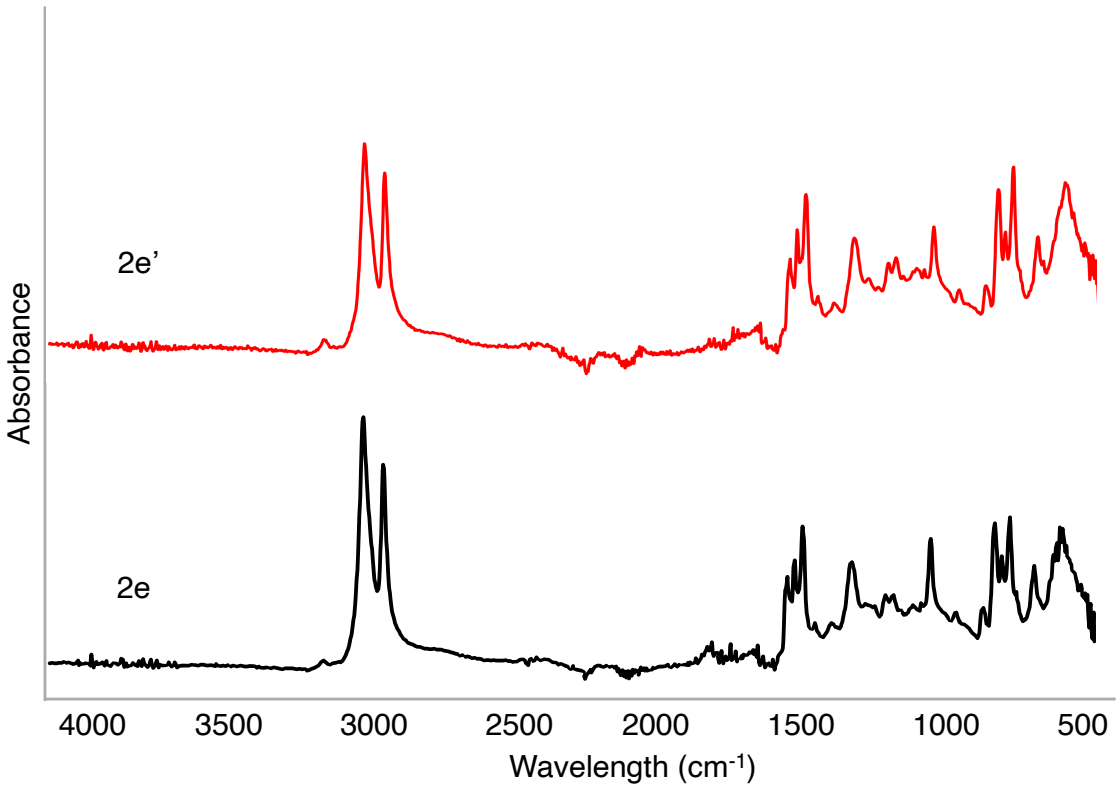


**Fig. S17** IR spectrum of Table S2, Entry 2e and 2e' with the $NaHCO_2$ H source.

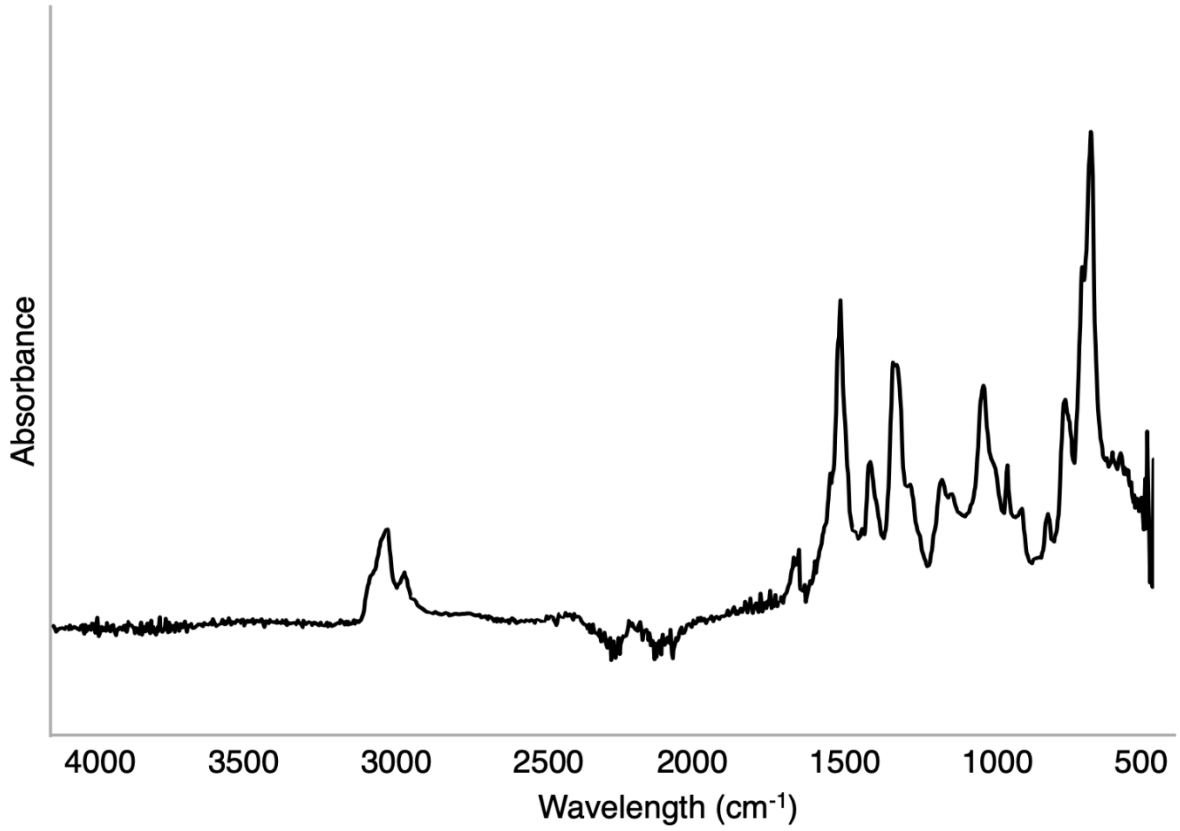


**Fig. S18** IR spectrum of Table S2, Entry 3a with the NaH H source.

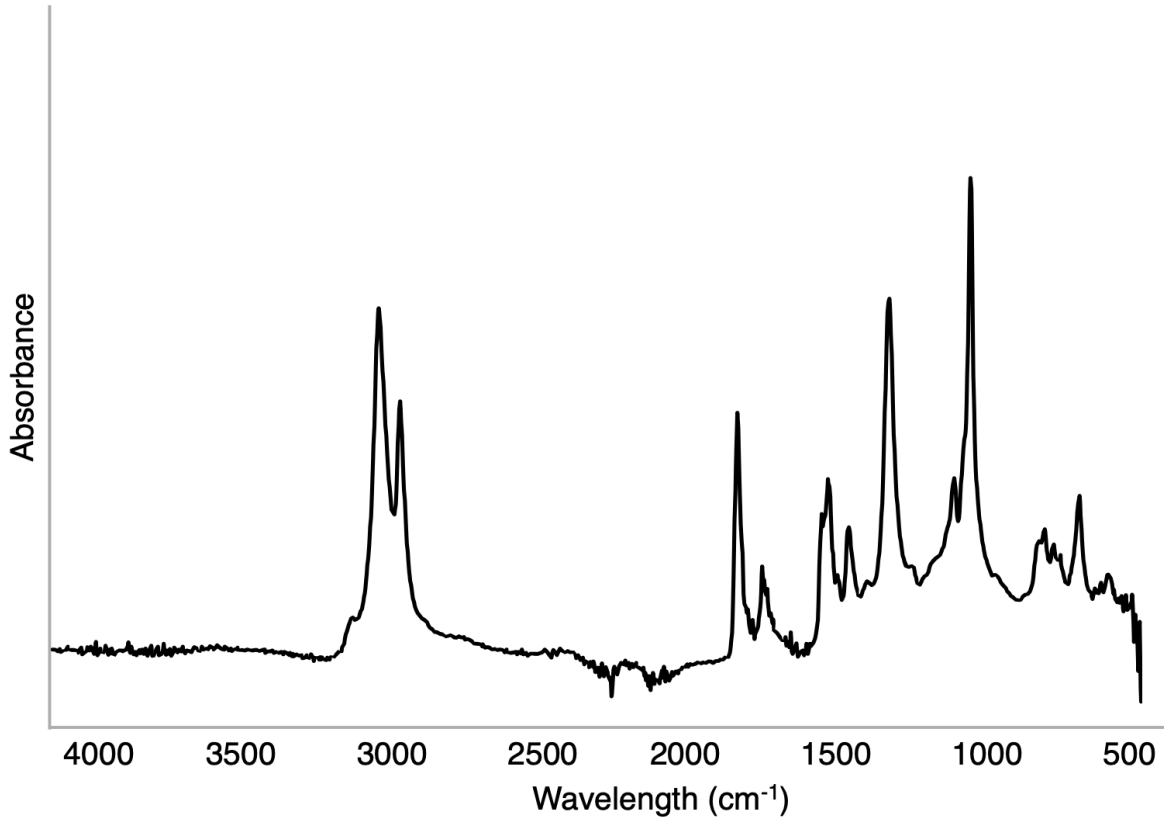


**Fig. S19** IR spectrum of Table S2, Entry 3b with the NaH H source.

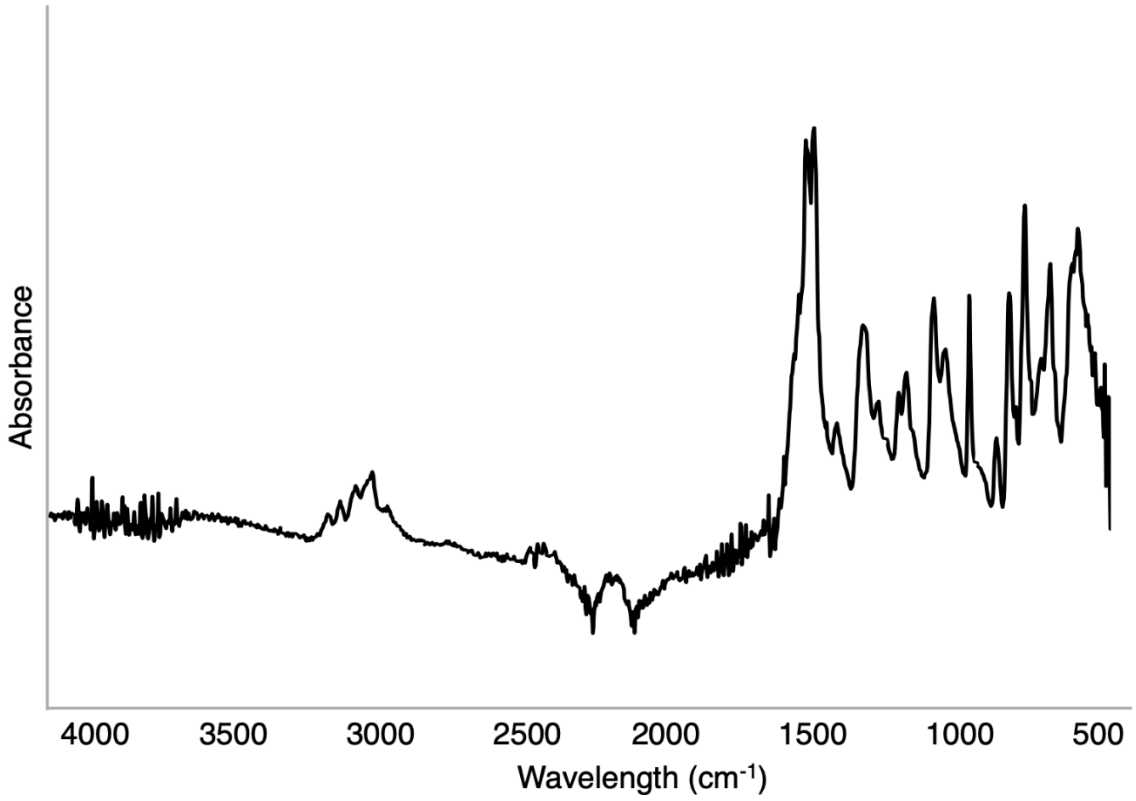


**Fig. S20** IR spectrum of Table S2, Entry 3c with the NaH H source.

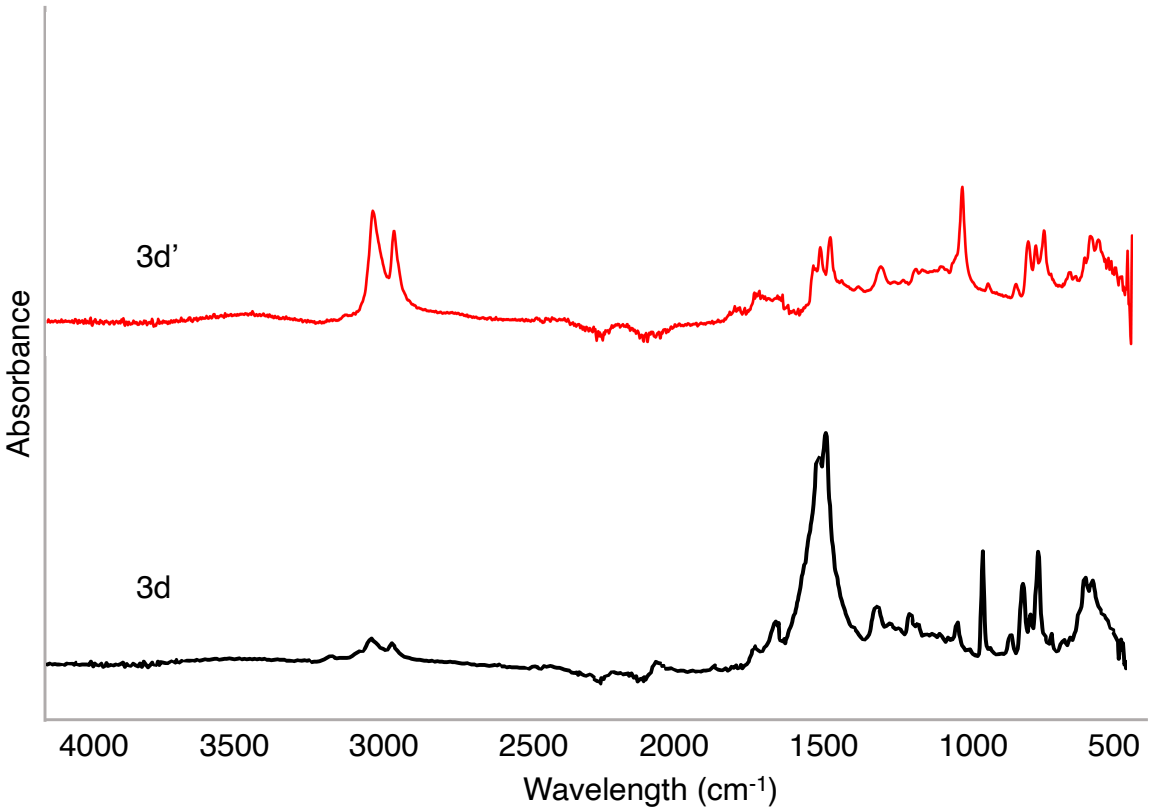


**Fig. S21** IR spectrum of Table S2, Entry 3d and 3d' with the NaH H source.

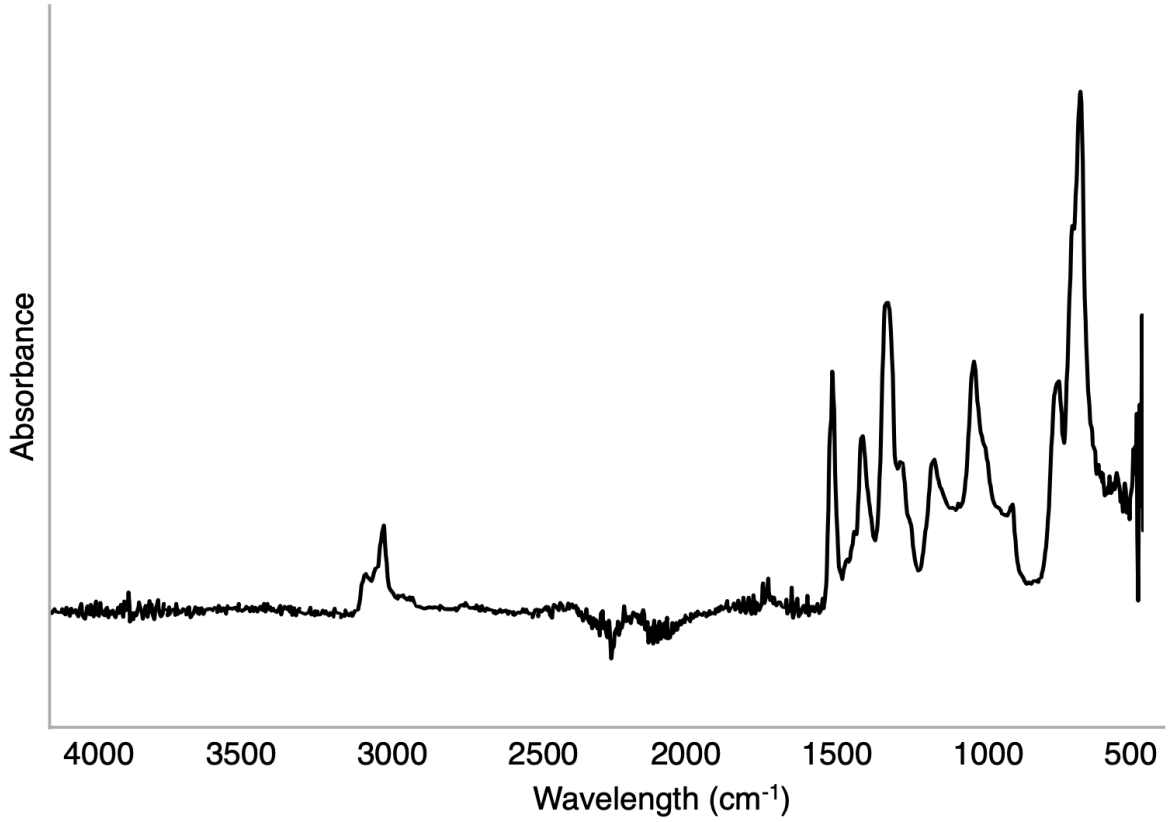


**Fig. S22** IR spectrum of Table S3, Entry 1a control reaction.

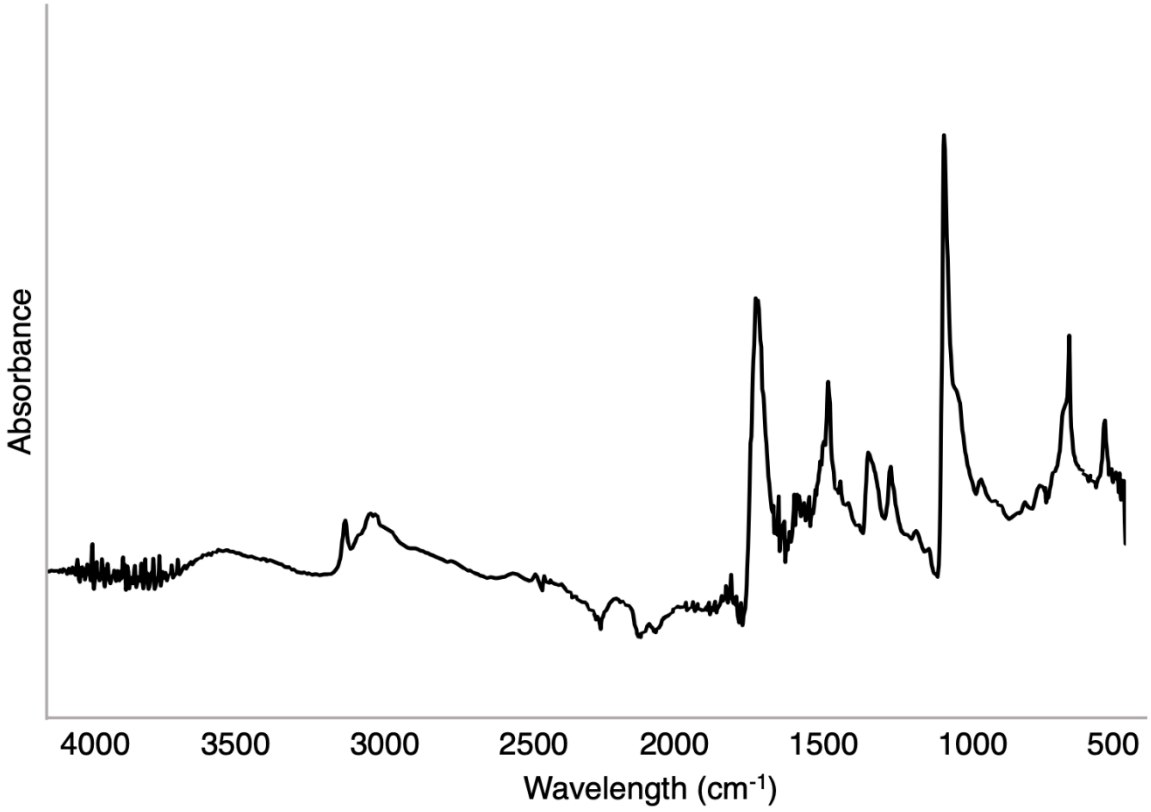


**Fig. S23** IR spectrum of Table S3, Entry 1b control reaction.

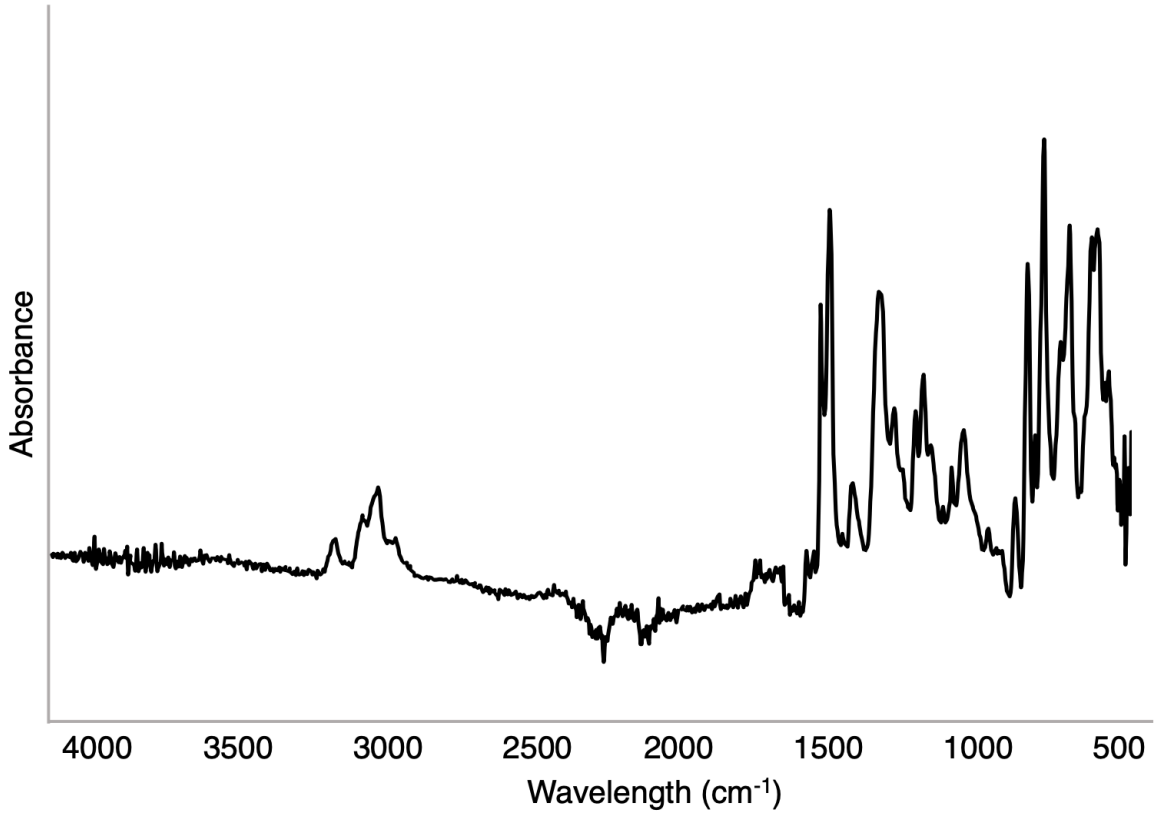


**Fig. S24** IR spectrum of Table S3, Entry 1c control reaction.

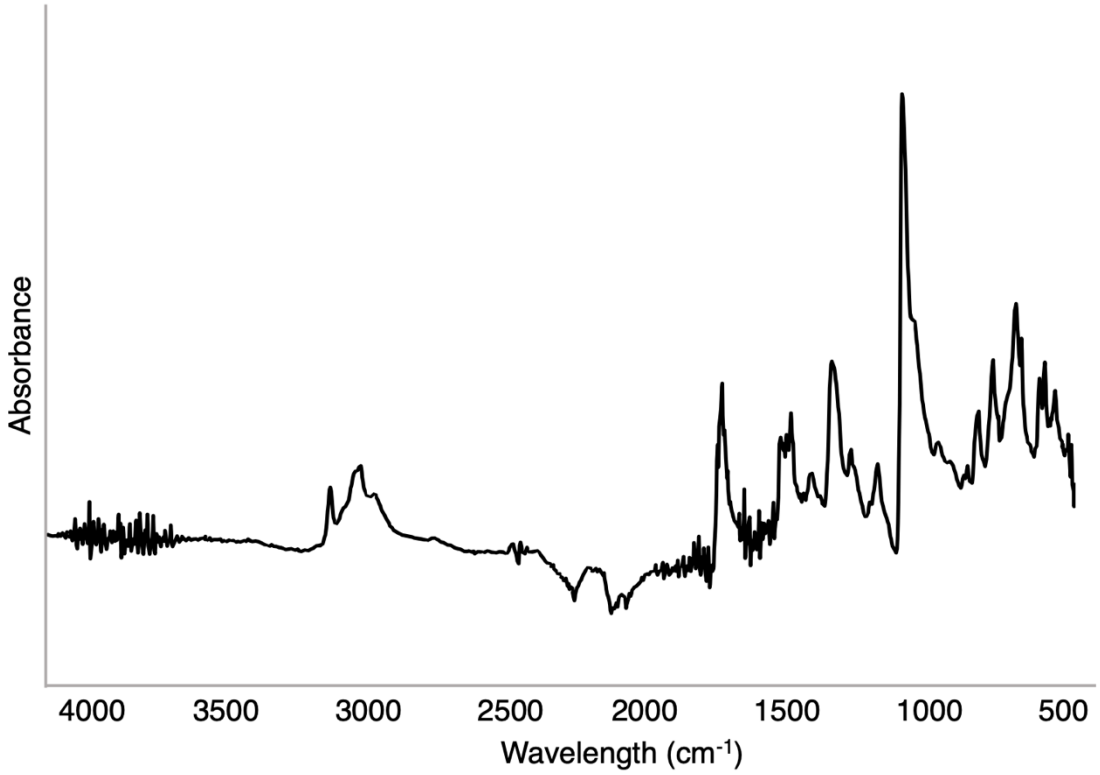


**Fig. S25** IR spectrum of Table S3, Entry 1d control reaction.

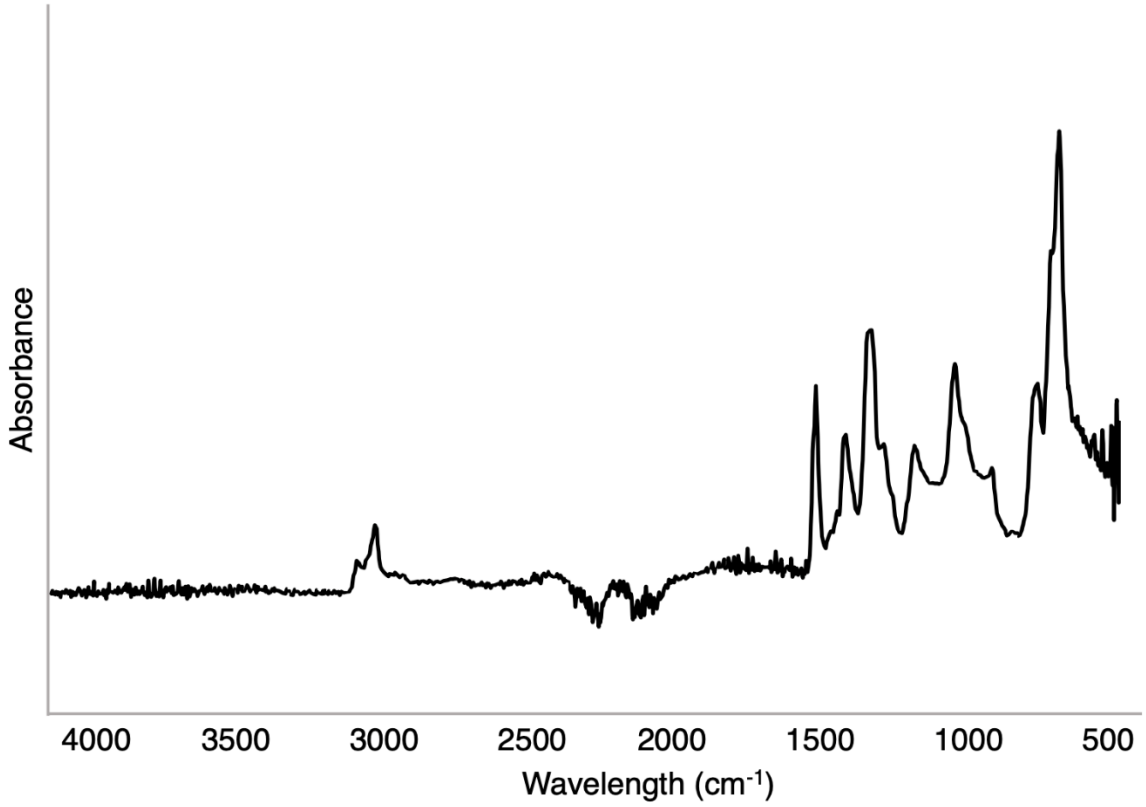


**Fig. S26** IR spectrum of Table S3, Entry 2a control reaction.

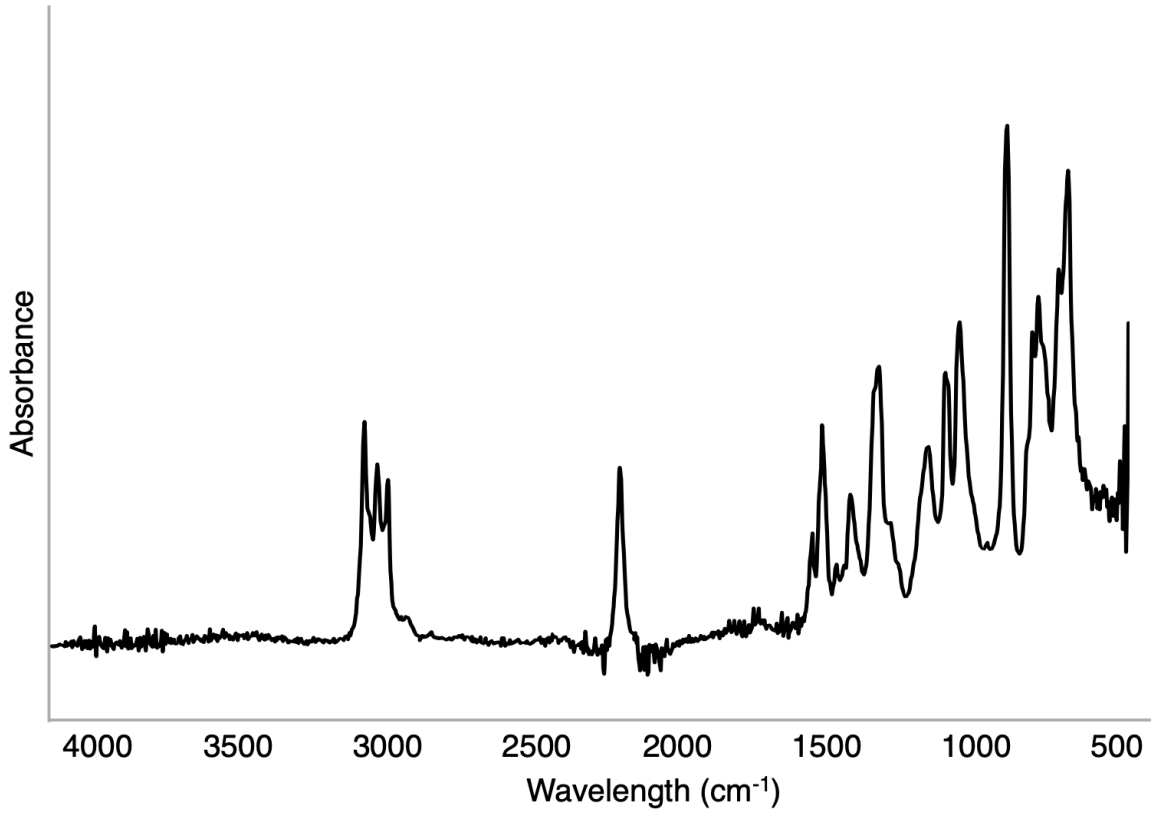


**Fig. S27** IR spectrum of Table S3, Entry 2b control reaction.

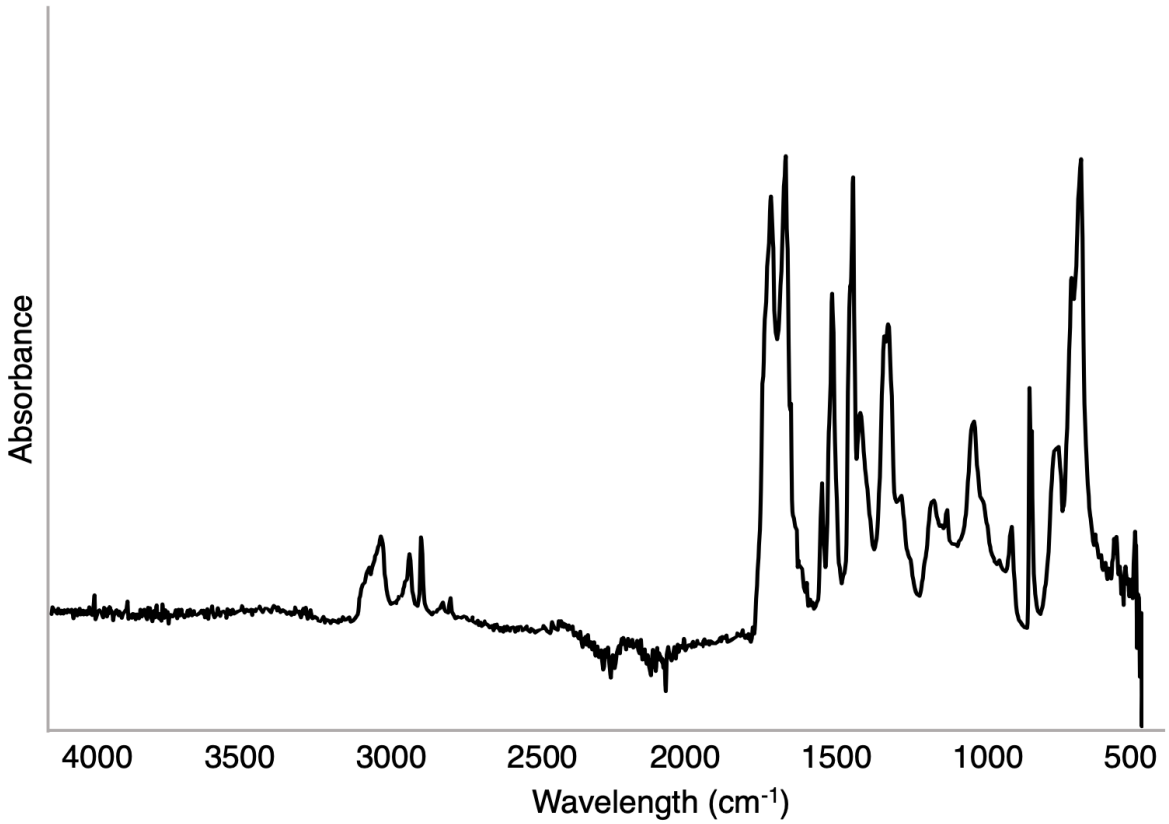


**Fig. S28** IR spectrum of Table S3, Entry 3a control reaction.

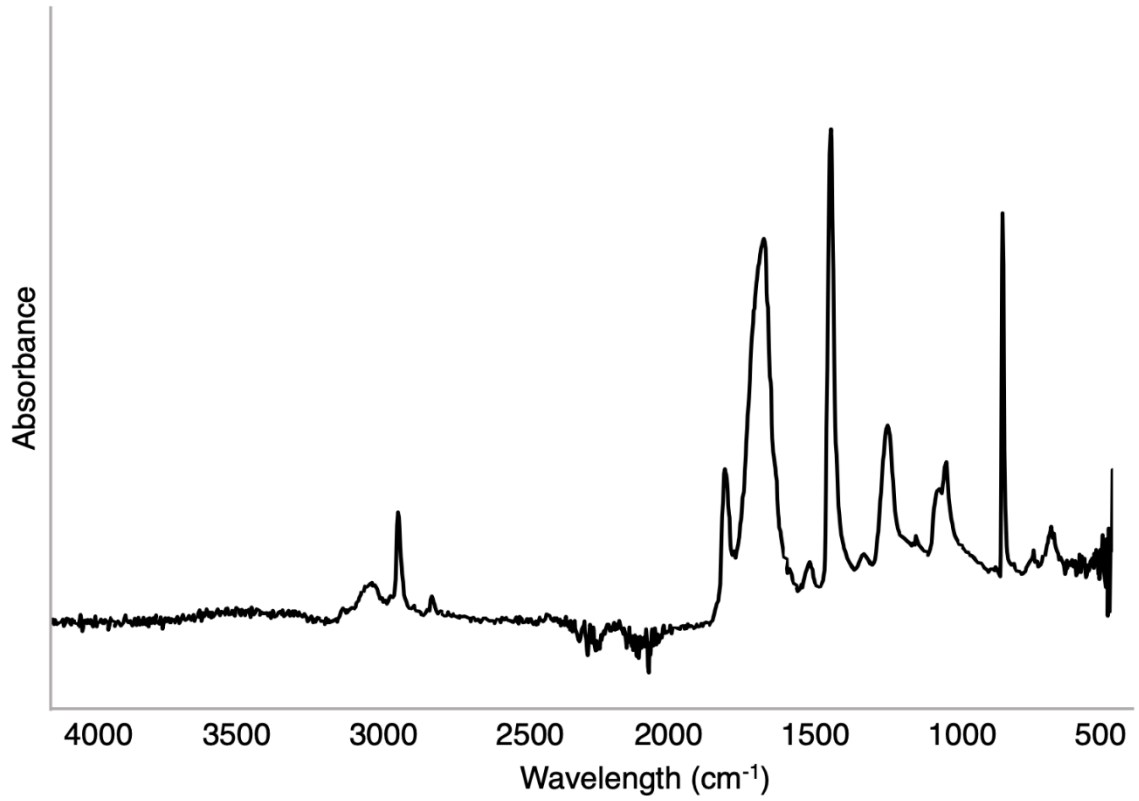


**Fig. S29** IR spectrum of Table S3, Entry 3b control reaction.

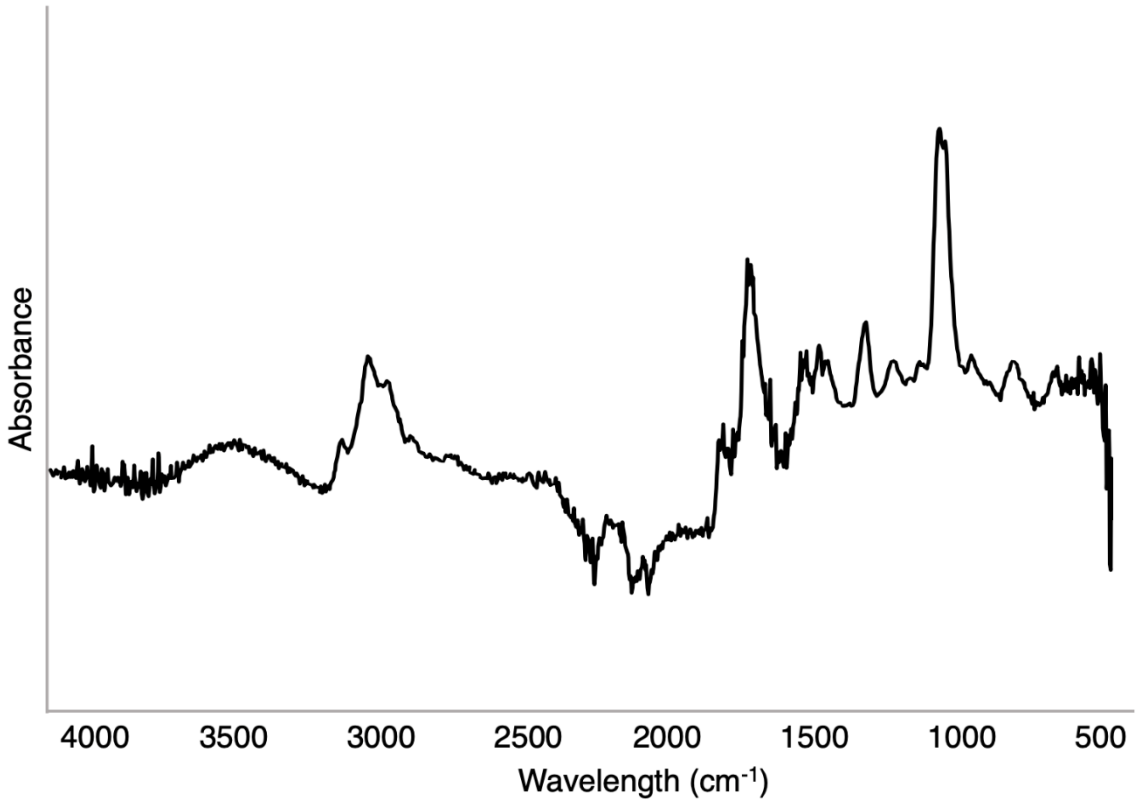


**Fig. S30** IR spectrum of Table S3, Entry 4a control reaction.

\

## 7. NMR Spectroscopy

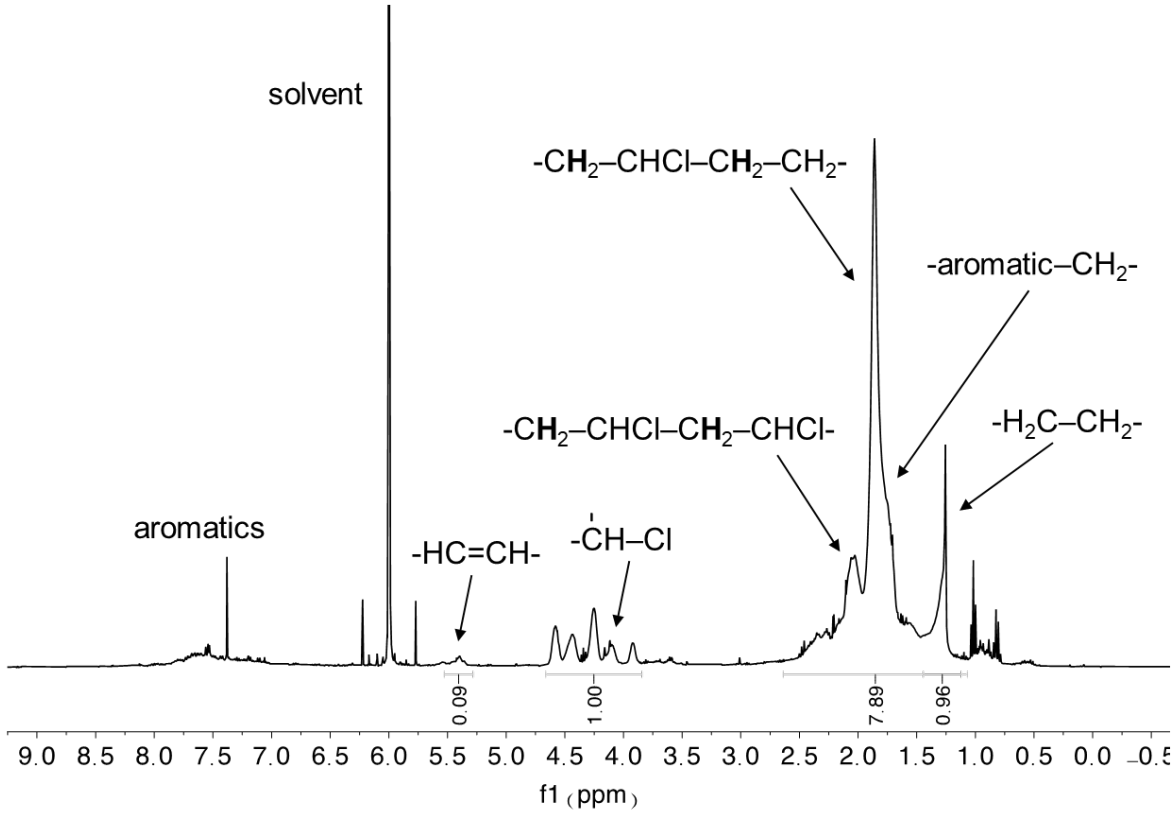


**Fig. S31** $^{1}$H NMR spectrum of the polymer product from Table S2, entry 1a with $Et_3SiH$.

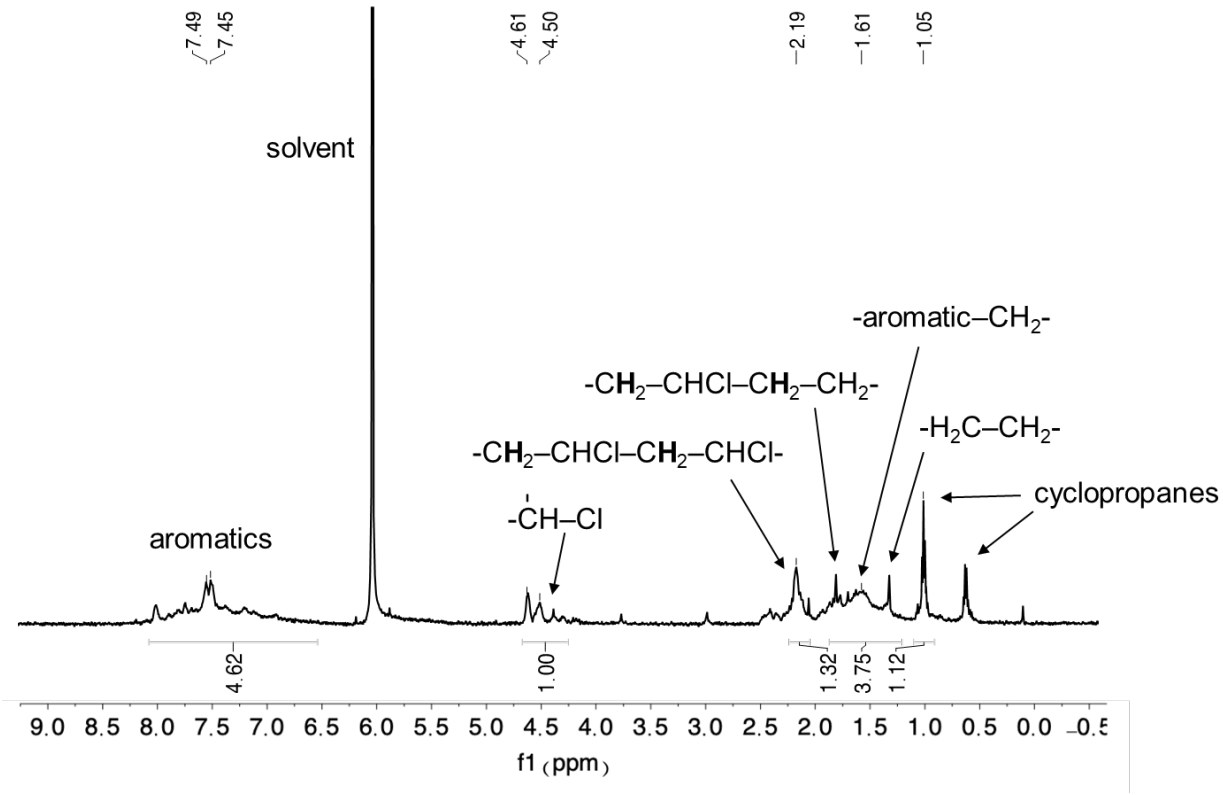


**Fig. S32** $^{1}$H NMR spectrum of the polymer product from Table S2, entry 1d' with $Et_3SiH$. Peaks between 0.5-1 ppm are attributed to cyclopropane rings on the basis of previous NMR assignments.[10,11]

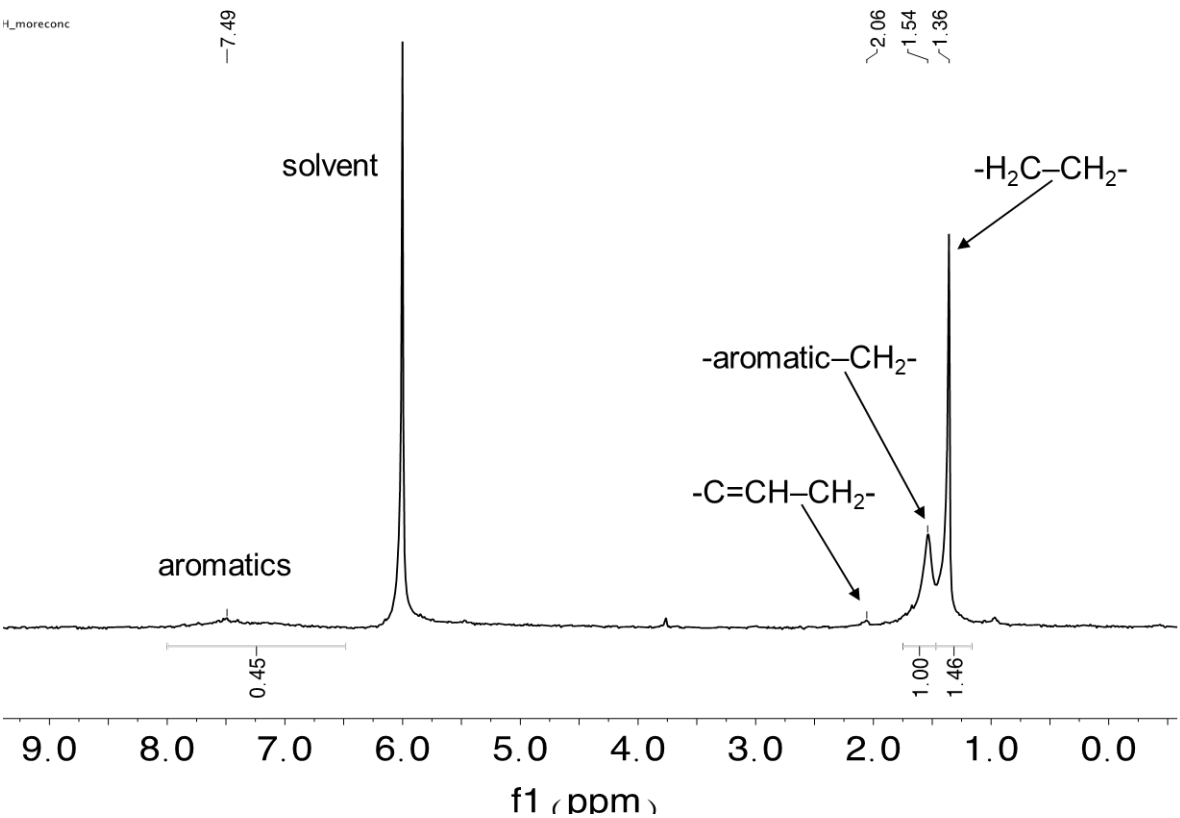


**Fig. S33** $^{1}$H NMR spectrum of polymer product from Table S2, entry 2c' with $NaHCO_2$.

Analogous NMR for Table S2, entry 2c can be found in the main manuscript.

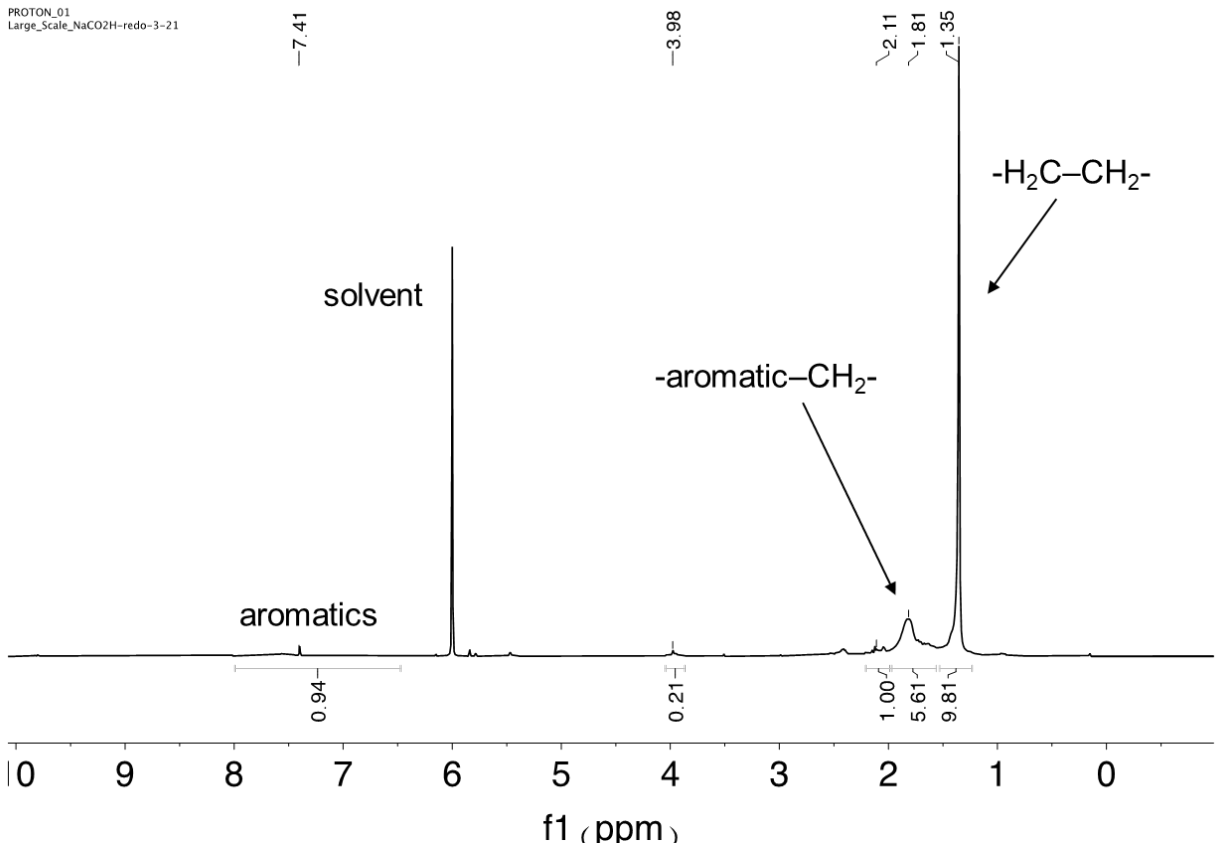


**Fig. S34** $^{1}$H NMR spectrum of the polymer product from Table S2, entry 2c" with $NaHCO_2$.

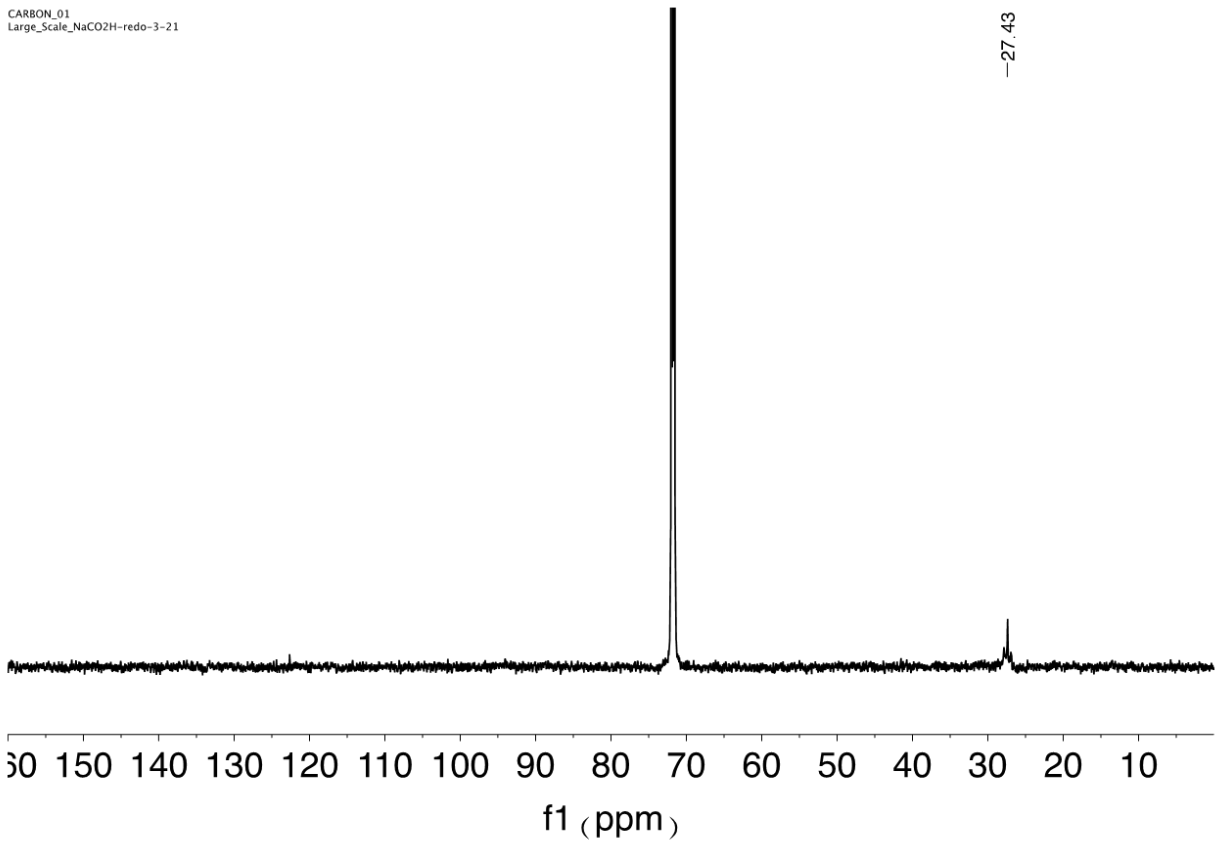


**Fig. S35** $^{13}C\{^{1}H\}$ NMR spectrum of the polymer product from Table S2, entry 2c" with $NaHCO_2$.

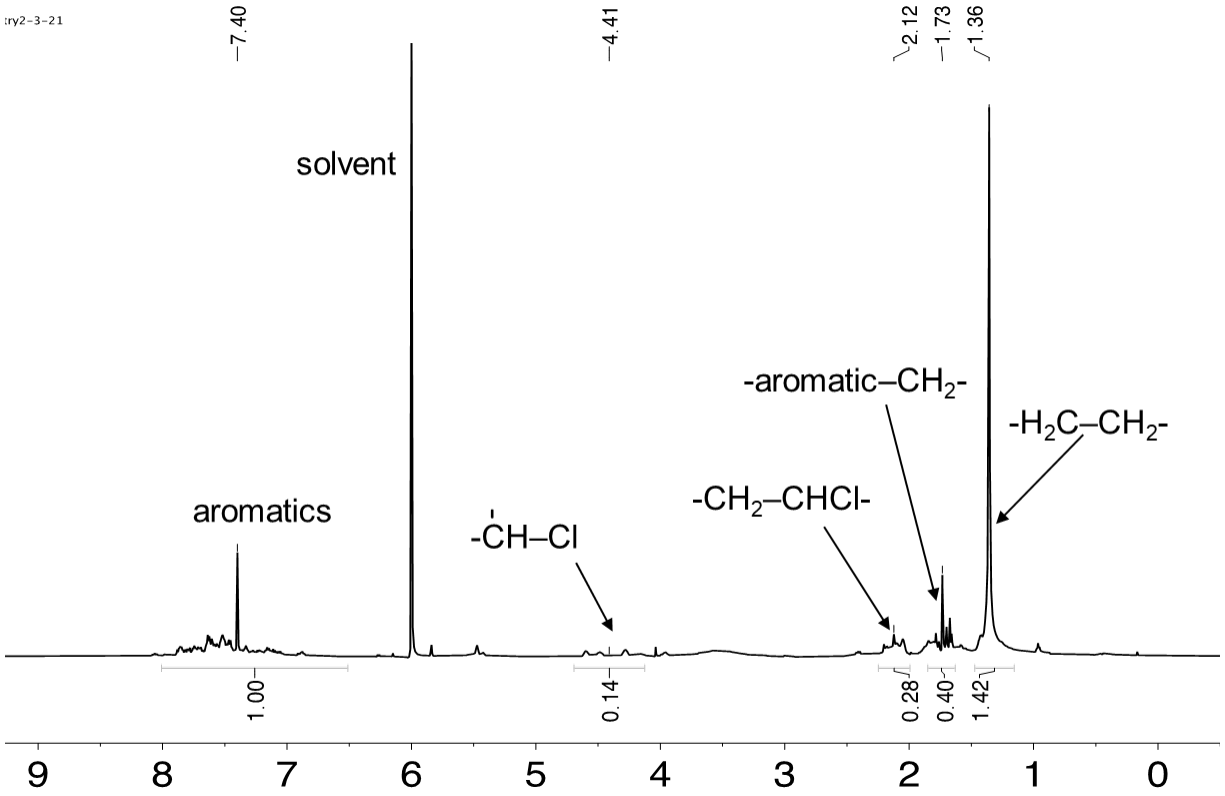


**Fig. S36** $^{1}$H NMR spectrum of the polymer product from Table S2, entry 2e' with $NaHCO_2$.

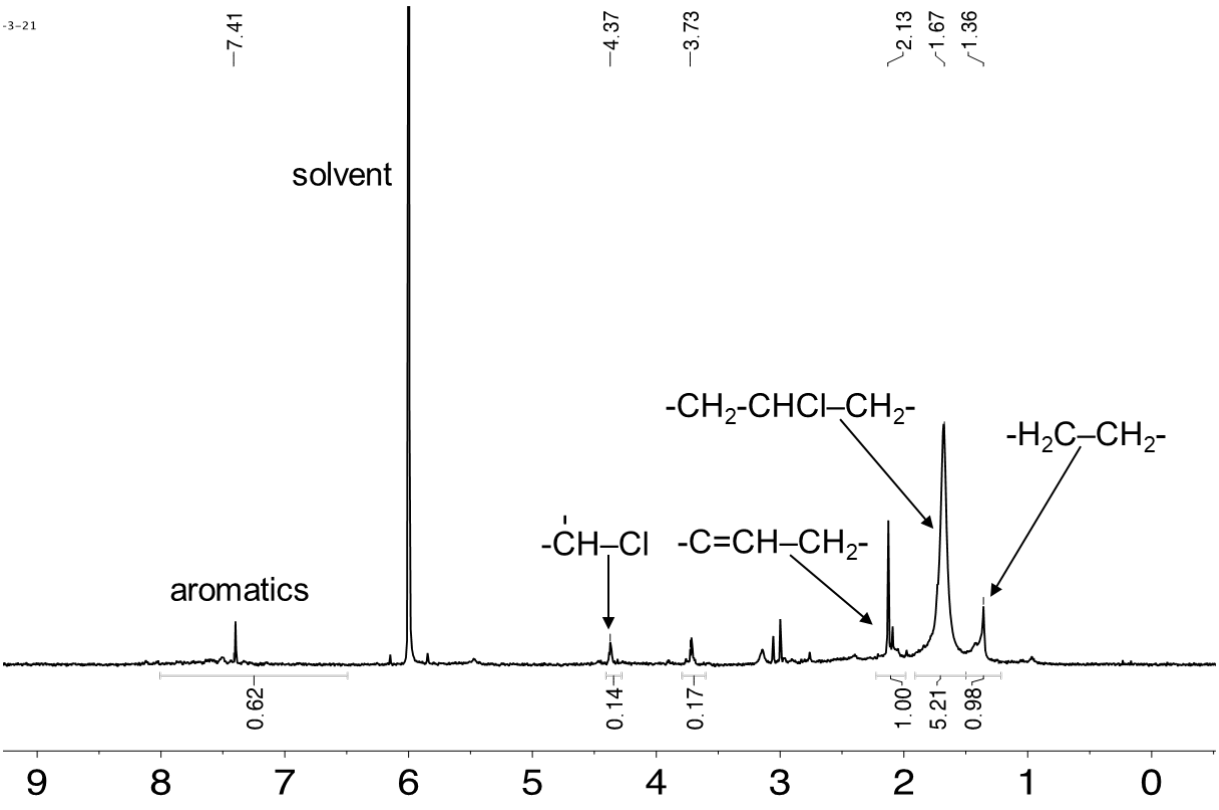


**Fig. S37** $^{1}$H NMR spectrum of polymer product from Table S2, entry 3b with NaH.

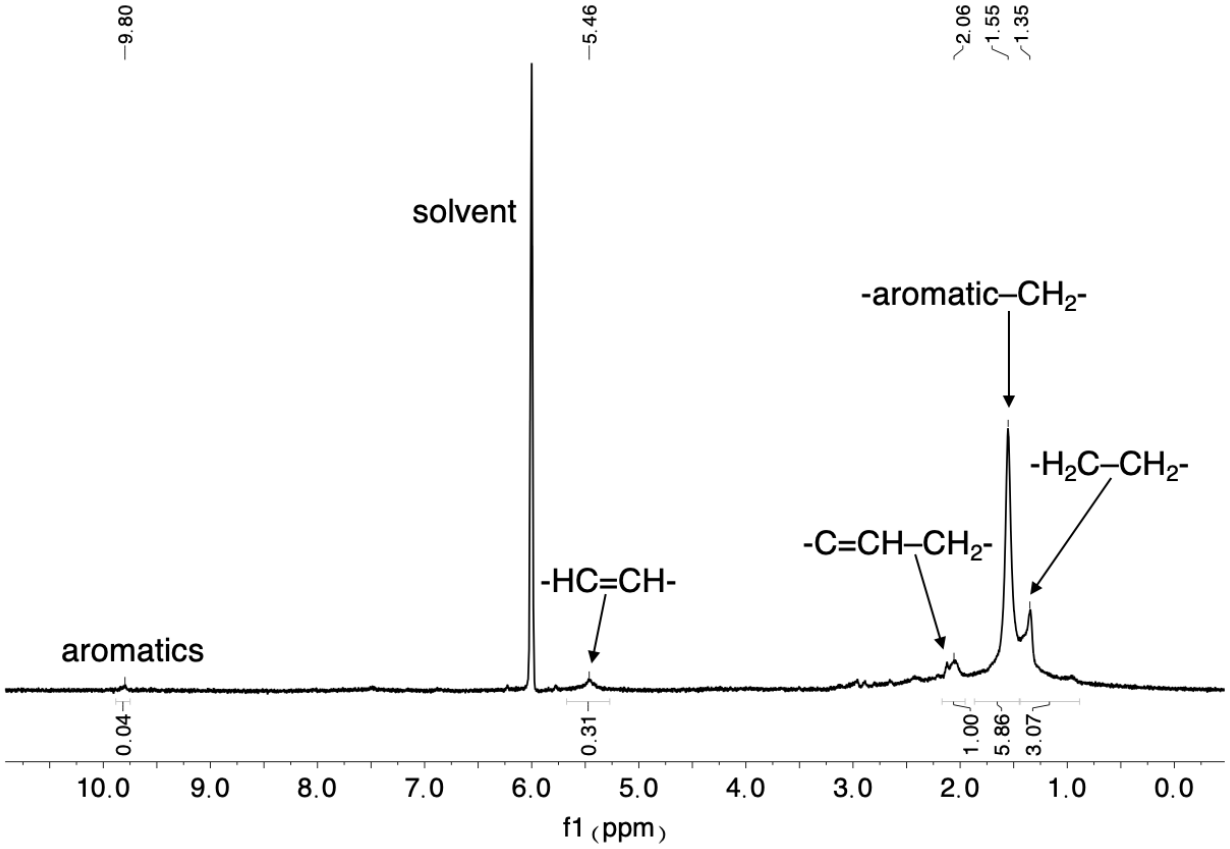


**Fig. S38** $^{1}$H NMR spectrum of polymer product from Table S2, entry 3d with NaH.

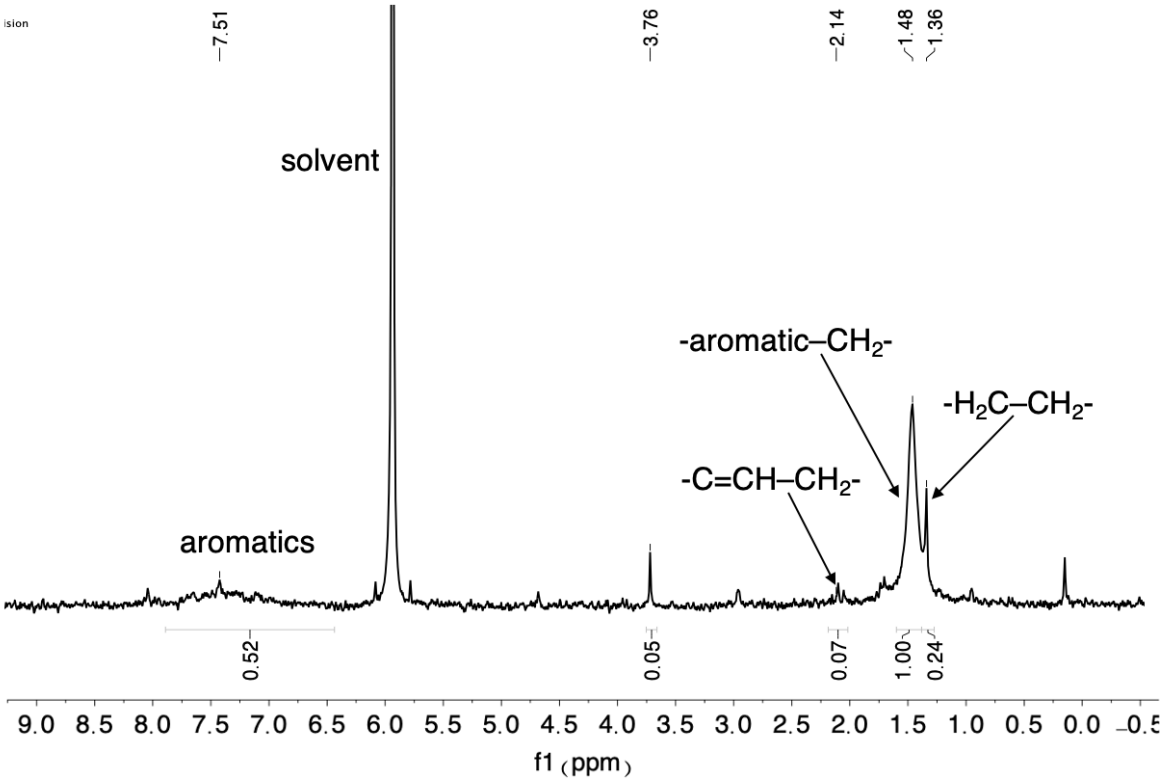


**Fig. S39** $^{1}$H NMR spectrum of polymer product from Table S2, entry 3d' with NaH.

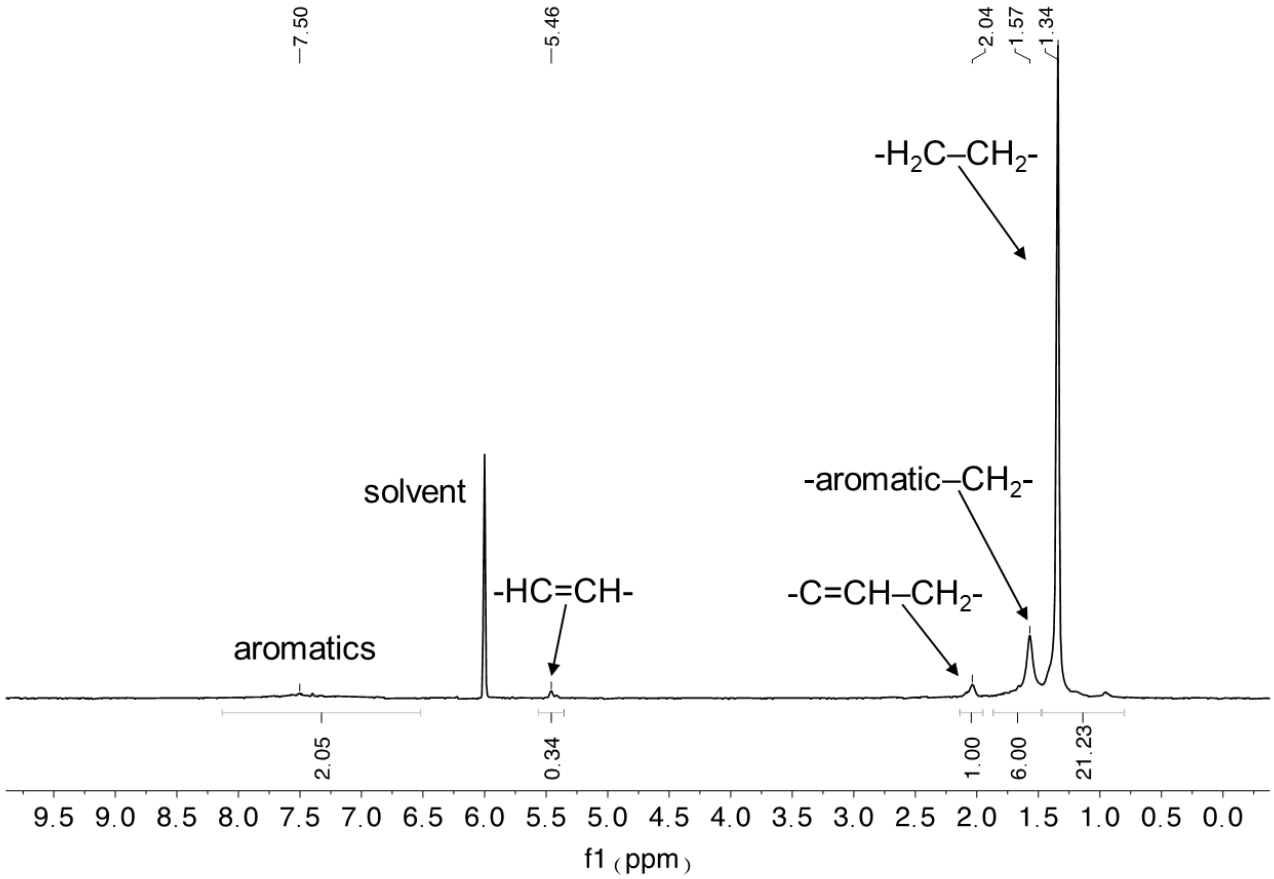


**Fig. S40** $^{1}$H NMR spectrum of polymer product from the toy lizard commercial PVC plastic reaction.

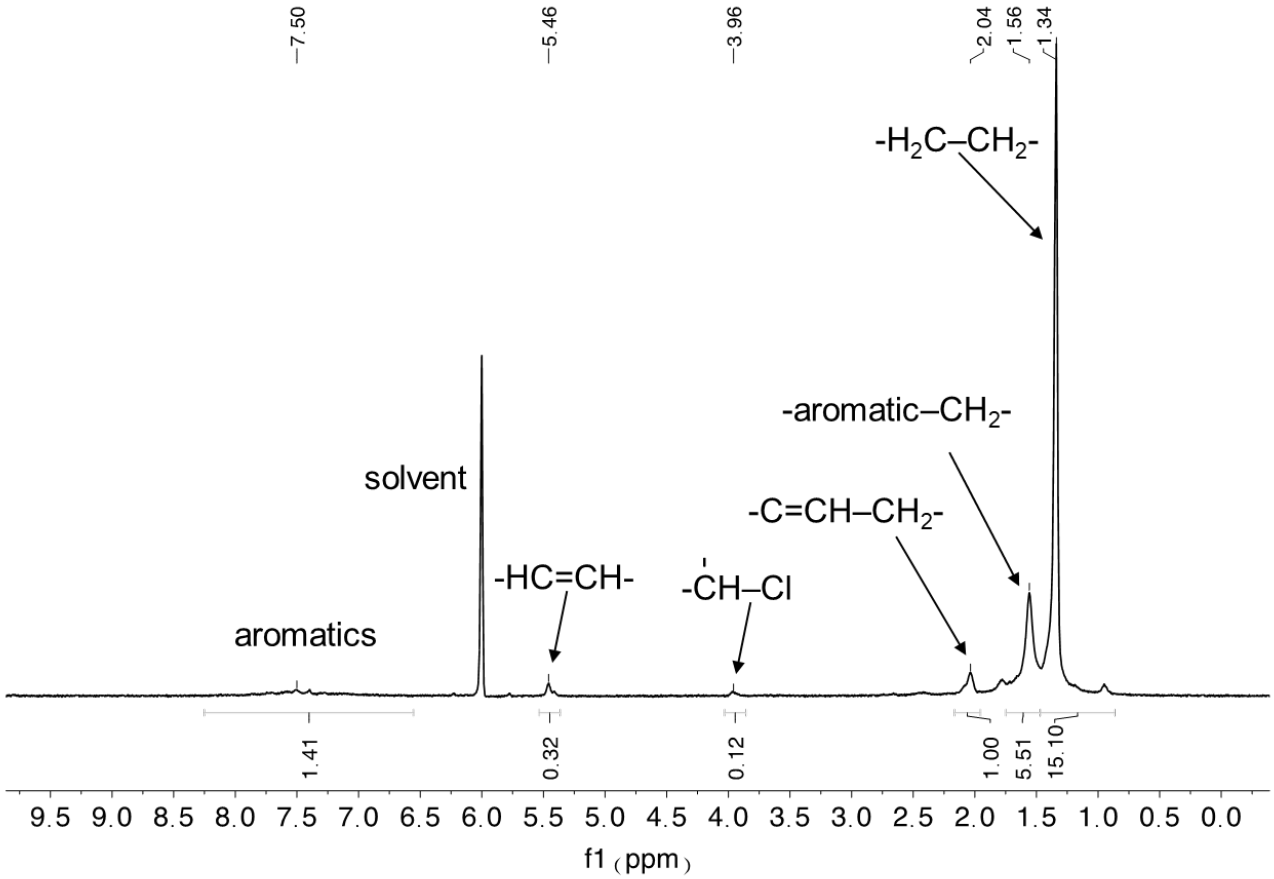


**Fig. S41** $^{1}$H NMR spectrum of polymer product from colorless PVC commercial bag reaction.

## 8. Scanning Electron Microscopy-Energy Dispersive X-Ray Spectroscopy (SEM-EDX)

Initial SEM and EDX measurements of the sodium formate reaction (Table S2, entry 2c) showing the highest HDC selectivity revealed consistent results across 12 spots on the sample. In one case, an impurity could easily be identified on the SEM image, with EDX revealing residual sodium formate as the likely impurity.

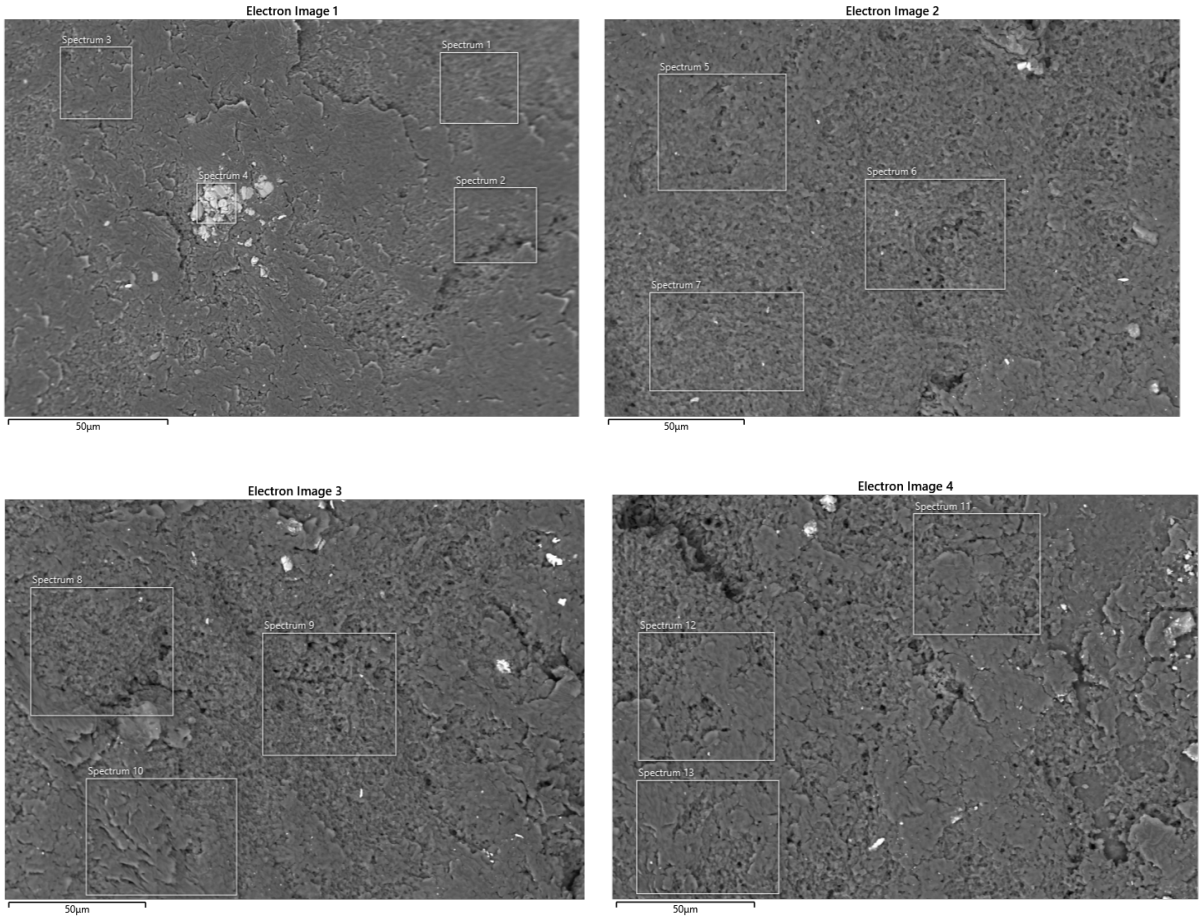


**Fig. S42** SEM images of EDX sample locations for the product from the optimized reaction with $NaHCO_2$ (Table S2, entry 2c) . Spectrum numbers correspond to sample numbers in Table S6. below.

**Table S5.** EDX data averaged over 12 sample locations and individual values for the product from the optimized reaction with $NaHCO_2$ (Table S2, entry 2c)

| | Atomic % | | | | | | | |
|---|---|---|---|---|---|---|---|---|
| | **C** | **O** | **F** | **Na** | **Si** | **P** | **Cl** | **Rh** |
| **Max** | 92.96 | 5.11 | 0.31 | 0.44 | 0.97 | 1.2 | 1 | 0.79 |
| **Min** | 91.56 | 3.54 | 0.12 | 0.2 | 0.22 | 1.03 | 0.79 | 0.65 |
| **Average** | 92.33 | 4.06 | – | 0.33 | 0.48 | 1.1 | 0.92 | 0.7 |
| **Standard Deviation** | 0.48 | 0.45 | – | 0.08 | 0.25 | 0.05 | 0.07 | 0.05 |

**Table S6.** EDX data for each sample location for the product from the optimized reaction with $NaHCO_2$ (Table S2, entry 2c)[a]

| **Sample #** | **1** | **2** | **3** | **5** | **6** | **7** | **8** | **9** | **10** | **11** | **12** | **13** |
|---|---|---|---|---|---|---|---|---|---|---|---|---|
| **C** | 92.49 | 92.1 | 91.91 | 91.56 | 92.73 | 92.59 | 92.32 | 92.96 | 91.85 | 91.75 | 92.92 | 92.72 |
| **O** | 3.81 | 3.73 | 4.06 | 5.11 | 4.07 | 4.14 | 4.31 | 3.67 | 4.5 | 4.21 | 3.54 | 3.54 |
| **F** | – | – | – | – | – | 0.13 | – | 0.12 | 0.12 | 0.31 | 0.16 | 0.3 |
| **Na** | 0.3 | 0.25 | 0.32 | 0.2 | 0.23 | 0.23 | 0.42 | 0.39 | 0.44 | 0.38 | 0.36 | 0.38 |
| **Si** | 0.65 | 0.97 | 0.89 | 0.65 | 0.36 | 0.36 | 0.32 | 0.22 | 0.45 | 0.42 | 0.24 | 0.24 |
| **P** | 1.11 | 1.17 | 1.11 | 1.04 | 1.09 | 1.07 | 1.04 | 1.05 | 1.03 | 1.2 | 1.13 | 1.12 |
| **Cl** | 0.9 | 0.97 | 0.95 | 0.79 | 0.84 | 0.79 | 0.94 | 0.95 | 0.94 | 1 | 0.95 | 0.96 |
| **Rh** | 0.73 | 0.79 | 0.76 | 0.66 | 0.67 | 0.69 | 0.65 | 0.65 | 0.66 | 0.72 | 0.71 | 0.73 |
| **Total** | 100 | 100 | 100 | 100 | 100 | 100 | 100 | 100 | 100 | 100 | 100 | 100 |

[a]Sample 4 was taken of the white crystalline solid found in the polymer sample as shown in Fig. S33 above. There was excess Na and O present, showing that it was excess sodium formate from the reaction.

EDX measurements were done on the three duplicate reactions for each H source (Table S2, entries 1a', 2c' and 3d' for $Et_3SiH$, $NaHCO_2$ and NaH, respectively. Values for 9 locations across the sample were consistent for all three polymer products, therefore averages are compared in Table S7.

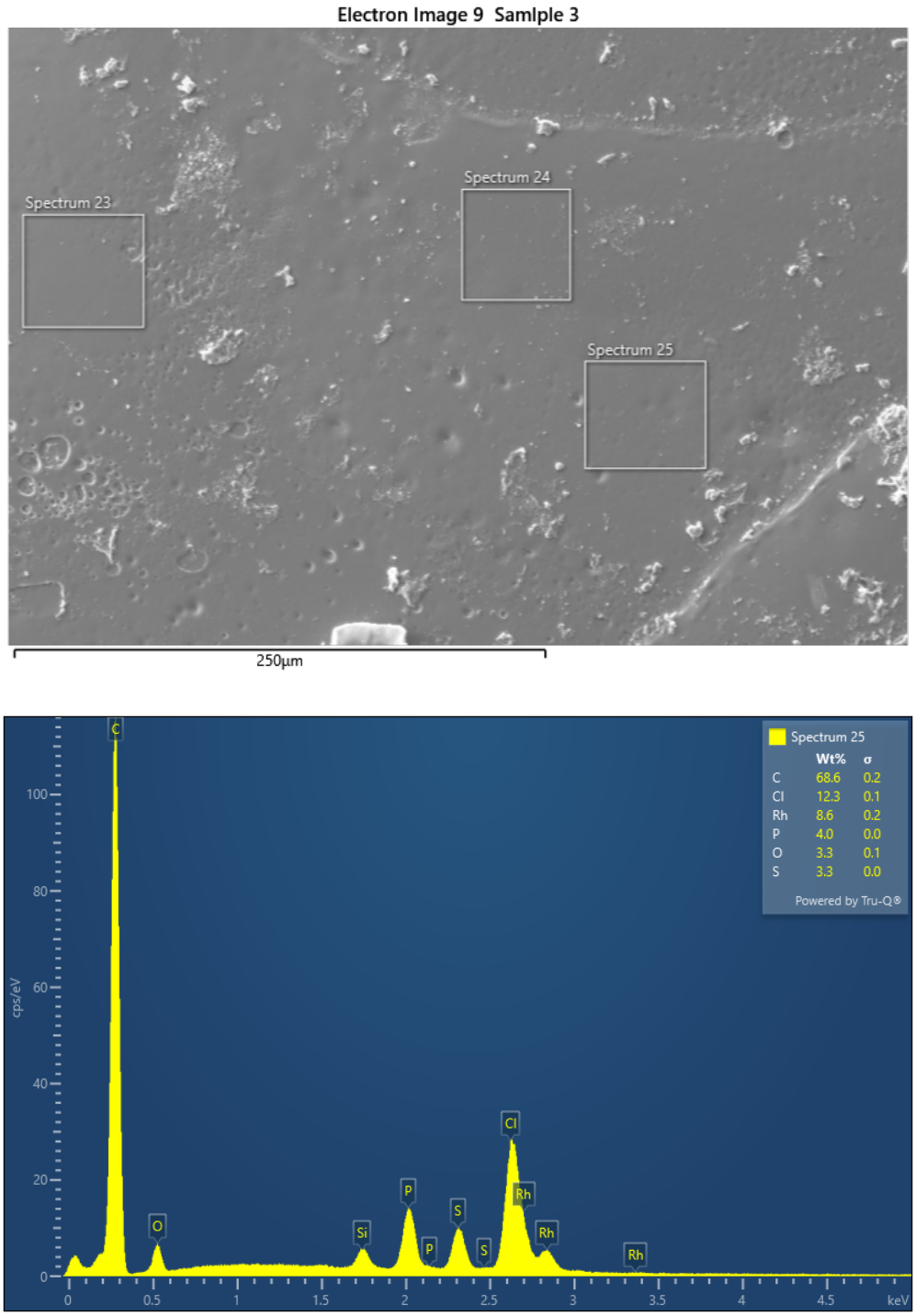


**Fig. S43** SEM image (top) and EDX spectrum (bottom) of the polymer product from the optimized reaction with $Et_3SiH$ (Table S2, entry 1a').

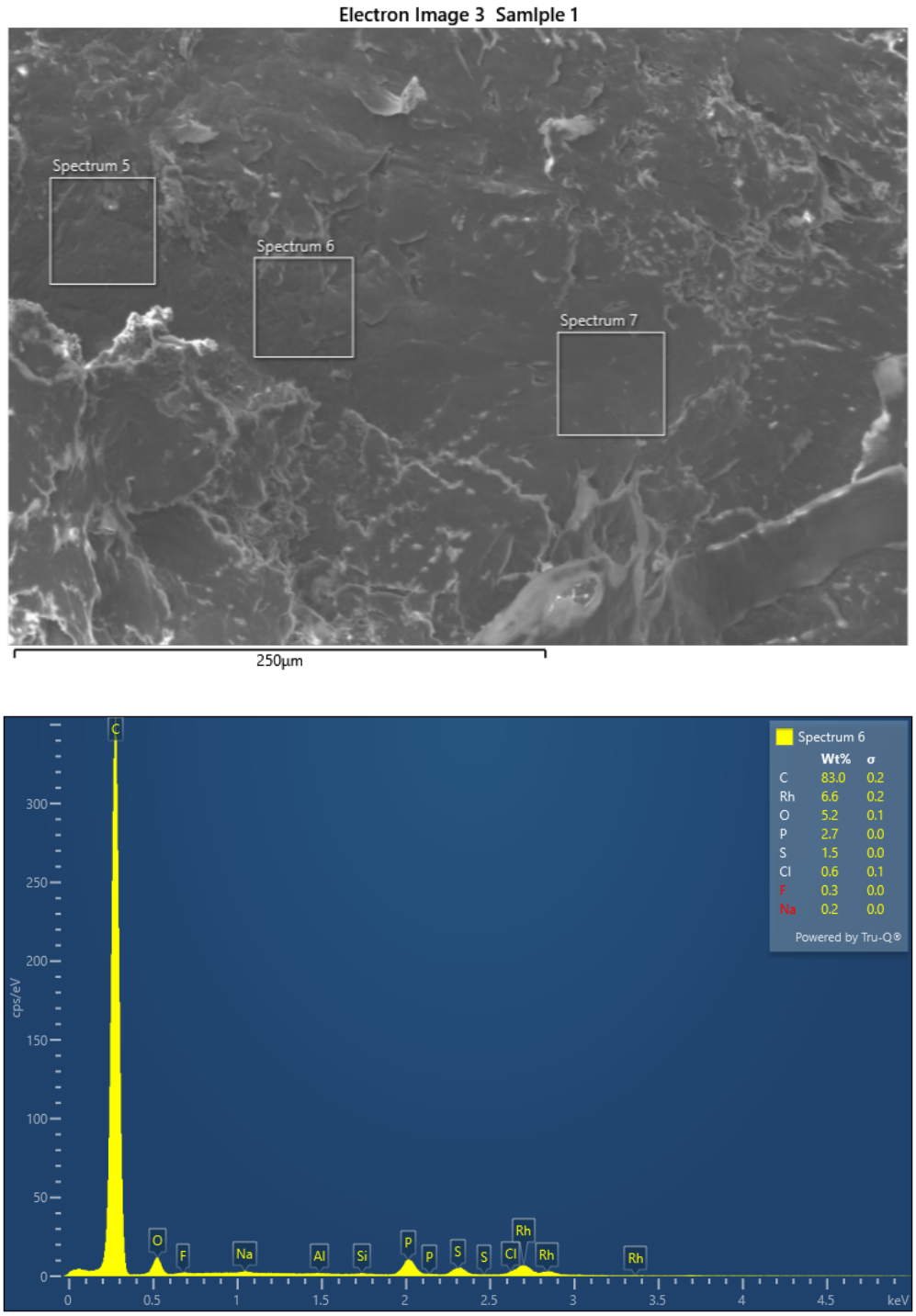


**Fig. S44** SEM image (top) and EDX spectrum (bottom) of the polymer product from the optimized reaction with $NaHCO_2$ (Table S2, entry 2c').

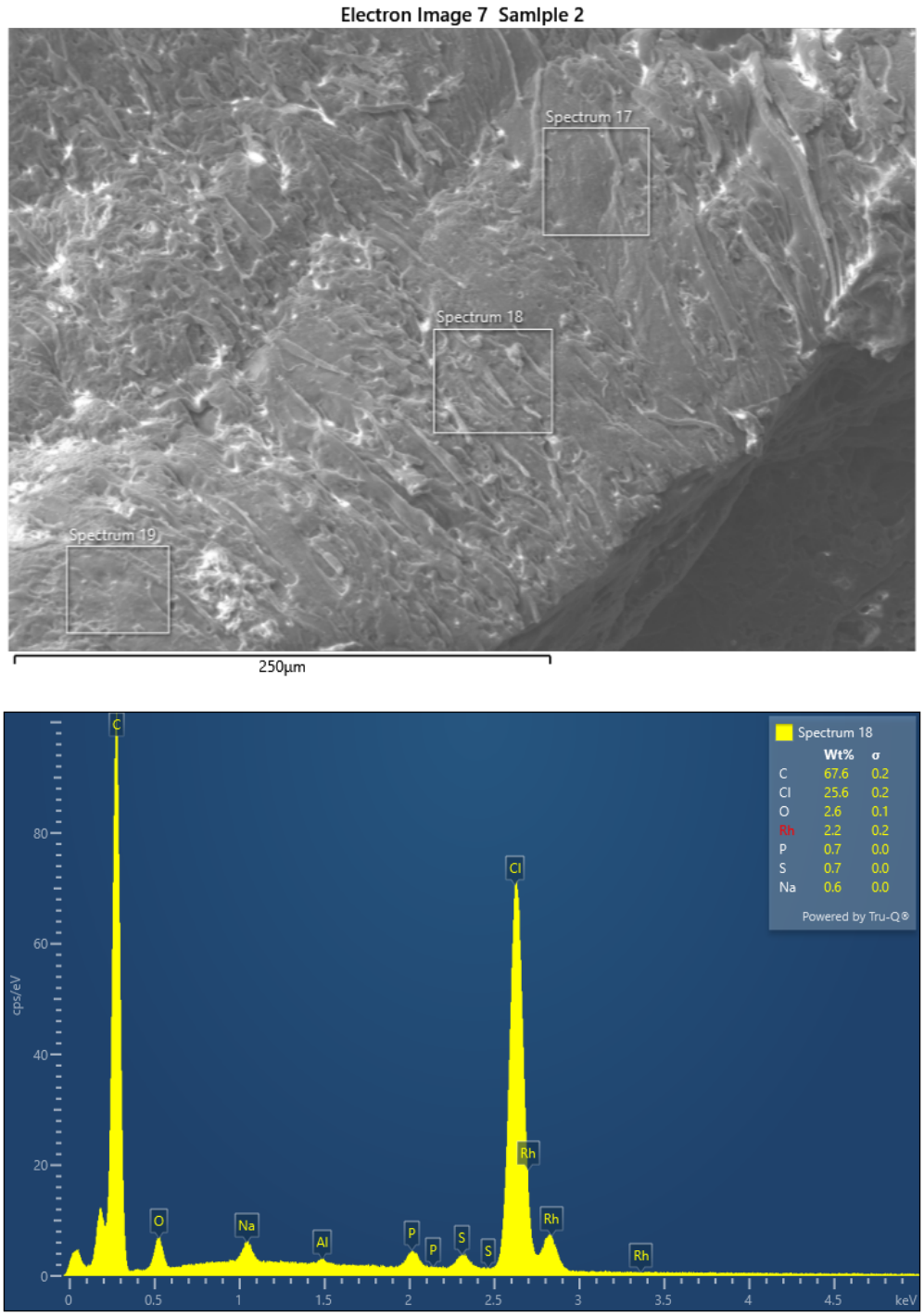


**Fig. S45** SEM image (top) and EDX spectrum (bottom) of the polymer product from the optimized reaction with NaH (Table S2, entry 3d').

**Table S7.** EDX data comparison of polymer products with different H sources.

| EDX | $Et_3SiH^a$ | | $NaHCO_2{}^b$ | | $NaHCO_2{}^{b'}$ | | $NaH^c$ | |
|---|---|---|---|---|---|---|---|---|
| **Element** | **Atomic %** | **Weight %** | **Atomic %** | **Weight %** | **Atomic %** | **Weight %** | **Atomic %** | **Weight %** |
| **C** | 87.9 | 71.5 | 92.3 | 82.6 | 92.3 | 83.2 | 82.3 | 62.8 |
| **O** | 2.7 | 3.0 | 4.2 | 5.0 | 4.1 | 4.9 | 2.2 | 2.2 |
| **F** | – | – | 0.3 | 0.4 | – | – | – | – |
| **Na** | – | – | 0.2 | 0.3 | 0.3 | 0.5 | 0.8 | 1.1 |
| **Si** | – | – | – | – | 0.5 | 1.1 | – | – |
| **P** | 1.3 | 2.8 | 1.2 | 2.8 | 1.1 | 2.6 | 0.4 | 0.8 |
| **S** | 1.0 | 2.3 | 0.6 | 1.4 | – | – | 0.4 | 0.7 |
| **Cl** | 6.2 | 14.7 | 0.3 | 0.9 | 0.9 | 2.4 | 13.7 | 30.1 |
| **Rh** | 0.8 | 5.8 | 0.8 | 6.5 | 0.7 | 5.4 | 0.3 | 2.2 |

[a] refers to product from reaction in Table S2, entry 1a'. [b] refers to product from reaction in Table S2, entry 2c. [b'] refers to product from reaction in Table S2, entry 2c'. [c] refers to product from reaction in Table S2, entry 3d'.

## 9. Gel Permeation Chromatography

The GPC chromatogram of PVC before and after reaction with $NaHCO_2$ under optimized conditions was recorded. The GPC data indicate reasonable preservation of the dispersity of the starting PVC, but some reduction of its degree of polymerization. This could be due to chain scission events, or due to the varied hydrodynamic radius between PVC and PE, since the polymer molecular weights were calibrated against polystyrene standards. Therefore, we take the dispersity information to be most meaningful to indicate limited chain scission.

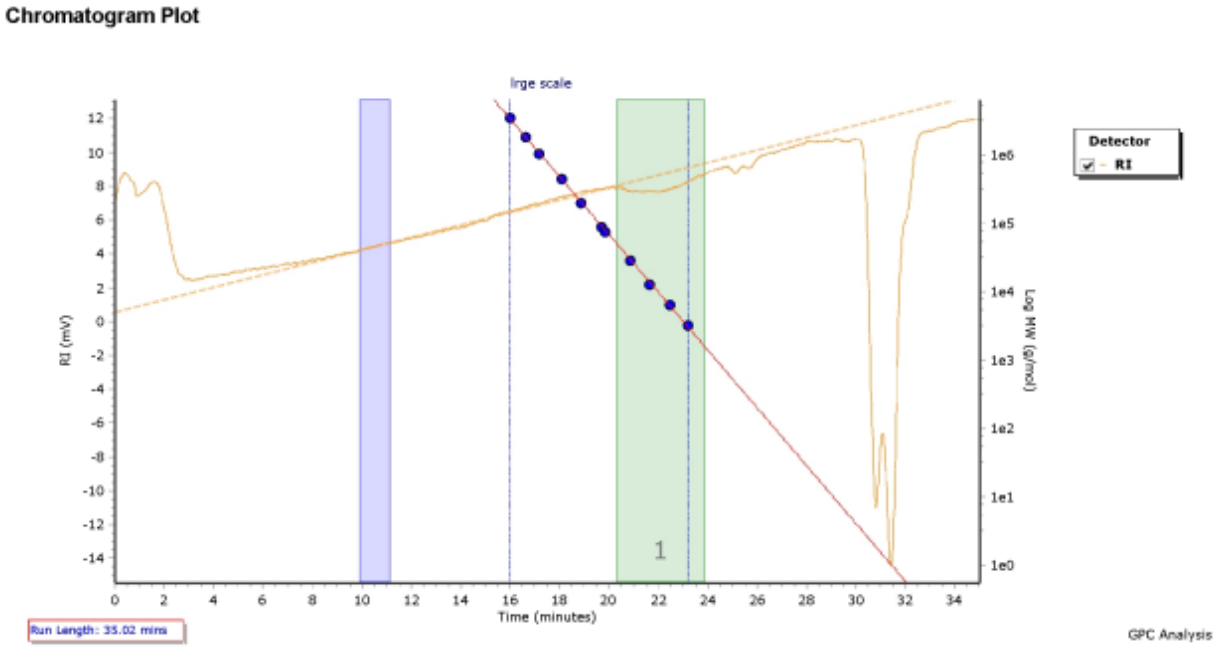


**Molecular Weight Averages**

| Peak | Mp (g/mol) | Mn (g/mol) | Mw (g/mol) | Mz (g/mol) | Mz+1 (g/mol) | Mv (g/mol) | PD |
|---|---|---|---|---|---|---|---|
| Peak 1 | 7190 | 5163 | 10683 | 19393 | 27067 | 18175 | 2.069 |

**Fig. S46** GPC data for polymer product from optimized reaction with $NaHCO_2$ (Table S2, entry 2c")

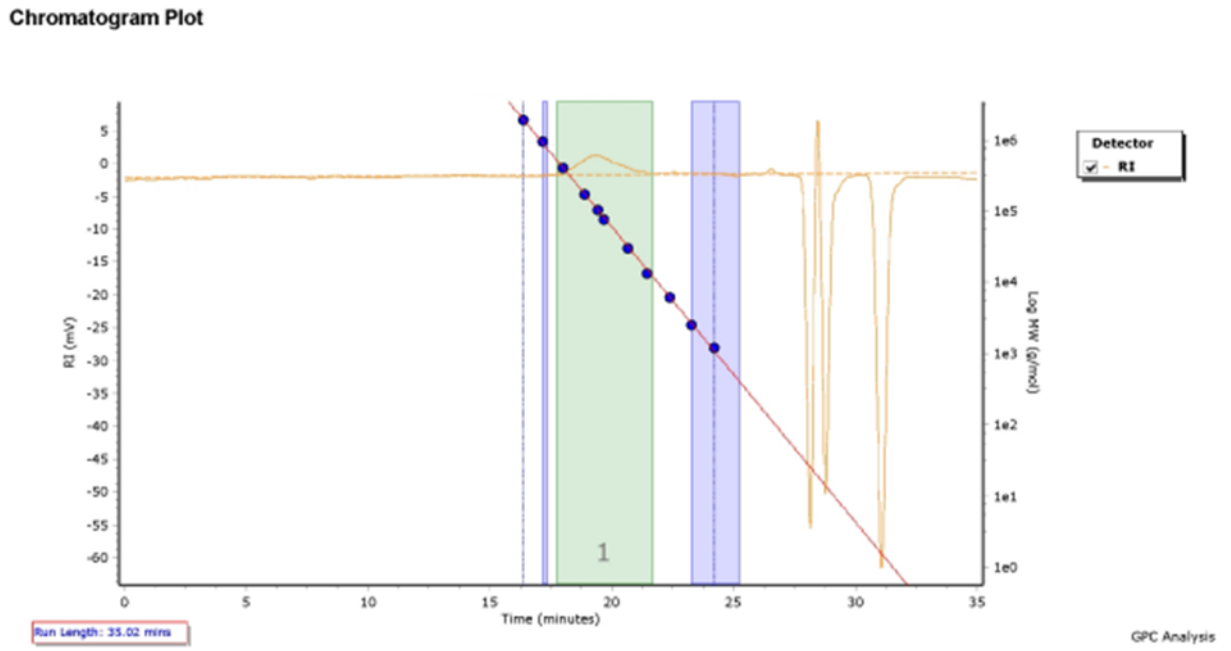


**Molecular Weight Averages**

| Peak | Mp (g/mol) | Mn (g/mol) | Mw (g/mol) | Mz (g/mol) | Mz+1 (g/mol) | Mv (g/mol) | PD |
|---|---|---|---|---|---|---|---|
| Peak 1 | 107513 | 67630 | 119152 | 181111 | 241277 | 172186 | 1.762 |

**Fig. S47** GPC data for low molecular weight PVC (CAS: 9002-86-2, Sigma Aldrich)

## 10. Thermogravimetric Analysis (TGA)

TGA of the polymer products from sodium formate reactions (Table S2, entries 2c and 2c') showed much higher thermal stability than PVC starting material and reactions with $Et_3SiH$ or NaH (Table S2, entries 1a' and 3d', respectively). The conditions with $Et_3SiH$ and NaH also show two distinct stages of mass loss, which could be due to dechlorination degree or dehydrochlorination. These results suggest that the sodium formate reactions lead to the most polyethylene-like polymers.

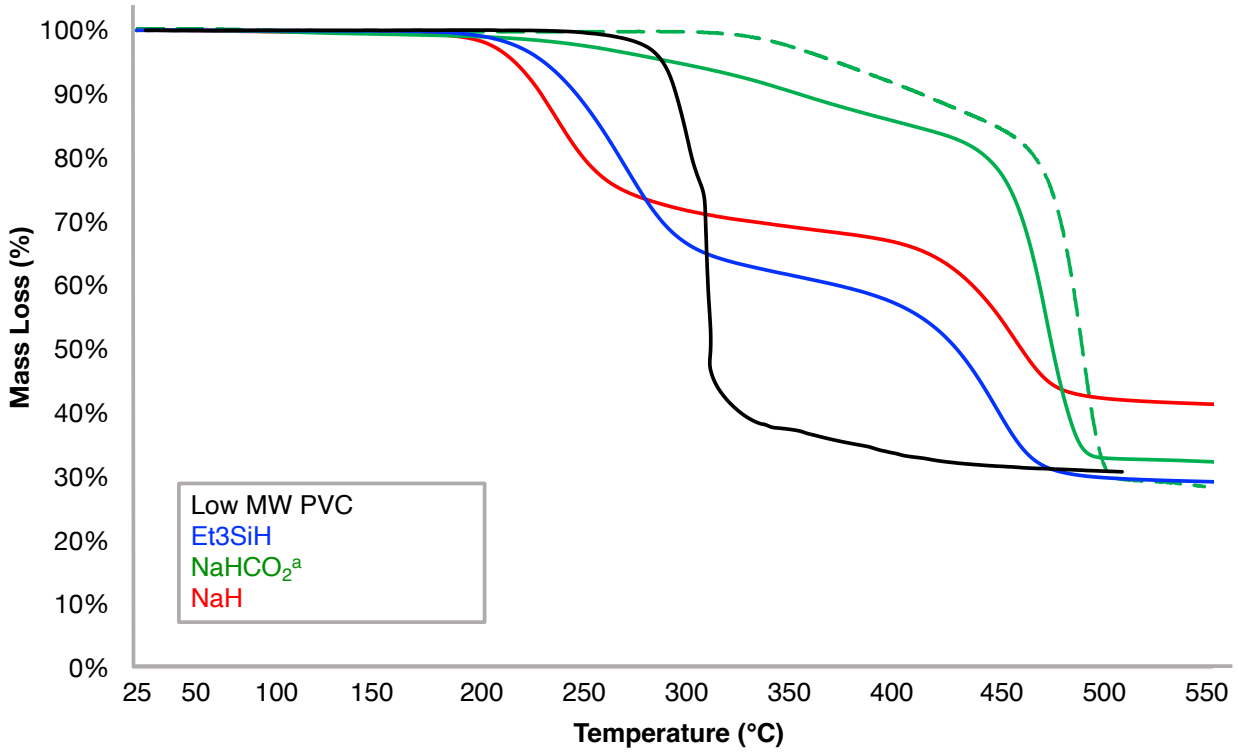


**Fig. S48** TGA of starting low molecular weight PVC and polymer products from selected samples: Table S2, entry 1a'; Table S2, entry 2c; Table S2, entry 2c'; Table S2, entry 3d'. [a]$NaHCO_2$ solid green trace shows Table S2, entry 2c', while the dashed trace shows Table S2, entry 2c.

## 11. Elemental Analysis, CHNS

**Table S8.** CHNS data of selected polymer products

| EA Data | % C | % H |
|---|---|---|
| **$Et_3SiH$ (Table S2, entry 1a)** | 57.5 | 8.4 |
| **$Et_3SiH$ (Table S2, entry 1a')** | 44.8 | 6.9 |
| **$Et_3SiH$ (Table S2, entry 1d')** | 45.3 | 5.0 |
| **$NaHCO_2$ (Table S2, entry 2c)** | 72.0 | 10.7 |
| **$NaHCO_2$ (Table S2, entry 2c')** | 74.2 | 11.5 |
| **$NaHCO_2$ (Table S2, entry 2c")** | 57.3 | 8.5 |
| **$NaHCO_2$ (Table S2, entry 2e')** | 59.7 | 8.5 |
| **NaH (Table S2, entry 3b)** | 70.5 | 8.4 |
| **NaH (Table S2, entry 3d')** | 52.2 | 6.9 |

## 12. Computational Methods and Models

The computational procedure for calculating reaction intermediates and transition structures is identical to that reported in our previous work.[12] All calculations are carried out using Version 5.3 (and higher) of Q-Chem ab initio quantum chemistry software.[13] Density functional theory (DFT) calculations with implicit solvation models are performed at the ωB97X-D/def2-SVP level of theory and the Karlsruhe def2-ECP effective core potential for heavy atoms.[14,15] Identical to our prior study, monochloropropane is chosen as the model substrate and the POP-pincer bound Rh(I) complex with P atoms coordinated to two methyl groups (instead of phenyl) is chosen as the model catalyst. Turnover frequencies are calculated using the energetic span model.[16]

### Role of solvent

Turnover frequencies (TOF) at 110°C for various solvents and salts are shown in Table S1.

**Table S9.** TOFs ($h^{-1}$) calculated at 110°C using the energetic span model and zero-point corrected electronic energies.

| Salt | NaHCO2 | | NaH | | SiHMe3 | |
|---|---|---|---|---|---|---|
| Solvent | THF | DMA | THF | DMA | THF | DMA |
| TOF | 5.84E-05 | 2.97E-04 | 2.53E-01 | 1.30E-01 | 2.53E-01 | 1.30E-01 |

## 13. References


1) SAINT+, 8.27B ed., *Bruker AXS* Madison, WI, 2011.
2) SADABS, 2012-1 ed., *Bruker AXS* Madison, WI, 2012.
3) G. M. Sheldrick, *Acta Crystallogr A Found Crystallogr*, 2008, **64**, 112–122.
4) G. M. Sheldrick, *Acta Crystallogr C Struct Chem*, 2015, **71**, 3–8.
5) G. M. Sheldrick, *Acta Crystallogr A Found Crystallogr*, 2015, **71**, 3–8.
6) SHELXL, Vol. 2012-4, 2012-1 ed.
7) T. J. Morrow, J. R. Gipper, W. E. Christman, N. Arulsamy and E. B. Hulley, *Organometallics*, 2020, **39**, 2356–2364.
8) M. A. Esteruelas, M. Oliván and A. Vélez, *Inorg. Chem.*, 2013, **52**, 5339–5349.
9) M. C. Haibach, D. Y. Wang, T. J. Emge, K. Krogh-Jespersen and A. S. Goldman, *Chem. Sci.*, 2013, **4**, 3683–3692.
10) R. E. Cais and C. P. Spencer, *European Polymer Journal*, 1982, **18**, 189–198.
11) D. T. Longone and A. H. Miller, *Chem. Commun. (London)*, 1967, 447.
12) S. Bac, M. E. Fieser and S. Mallikarjun Sharada, *Phys. Chem. Chem. Phys.*, 2022, **24**, 3518–3522.
13) E. Epifanovsky, A. T. B. Gilbert, X. Feng, J. Lee, Y. Mao, N. Mardirossian, P. Pokhilko, A. F. White, M. P. Coons, A. L. Dempwolff, Z. Gan, D. Hait, P. R. Horn, L. D. Jacobson, I. Kaliman, J. Kussmann, A. W. Lange, K. U. Lao, D. S. Levine, J. Liu, S. C. McKenzie, A. F. Morrison, K. D. Nanda, F. Plasser, D. R. Rehn, M. L. Vidal, Z.-Q. You, Y. Zhu, B. Alam, B. J. Albrecht, A. Aldossary, E. Alguire, J. H. Andersen, V. Athavale, D. Barton, K. Begam, A. Behn, N. Bellonzi, Y. A. Bernard, E. J. Berquist, H. G. A. Burton, A. Carreras, K. Carter-Fenk, R. Chakraborty, A. D. Chien, K. D. Closser, V. Cofer-Shabica, S. Dasgupta, M. de Wergifosse, J. Deng, M. Diedenhofen, H. Do, S. Ehlert, P.-T. Fang, S. Fatehi, Q. Feng, T. Friedhoff, J. Gayvert, Q. Ge, G. Gidofalvi, M. Goldey, J. Gomes, C. E. González-Espinoza, S. Gulania, A. O. Gunina, M. W. D. Hanson-Heine, P. H. P. Harbach, A. Hauser, M. F. Herbst, M. Hernández Vera, M. Hodecker, Z. C. Holden, S. Houck, X. Huang, K. Hui, B. C. Huynh, M. Ivanov, Á. Jász, H. Ji, H. Jiang, B. Kaduk, S. Kähler, K. Khistyaev, J. Kim, G. Kis, P. Klunzinger, Z. Koczor-Benda, J. H. Koh, D. Kosenkov, L. Koulias, T. Kowalczyk, C. M. Krauter, K. Kue, A. Kunitsa, T. Kus, I. Ladjánszki, A. Landau, K. V. Lawler, D. Lefrancois, S. Lehtola, R. R. Li, Y.-P. Li, J. Liang, M. Liebenthal, H.-H. Lin, Y.-S. Lin, F. Liu, K.-Y. Liu, M. Loipersberger, A. Luenser, A. Manjanath, P. Manohar, E. Mansoor, S. F. Manzer, S.-P. Mao, A. V. Marenich, T. Markovich, S. Mason, S. A. Maurer, P. F. McLaughlin, M. F. S. J. Menger, J.-M. Mewes, S. A. Mewes, P. Morgante, J. W. Mullinax, K. J. Oosterbaan, G. Paran, A. C. Paul, S. K. Paul, F. Pavošević, Z. Pei, S. Prager, E. I. Proynov, Á. Rák, E. Ramos-Cordoba, B. Rana, A. E. Rask, A. Rettig, R. M. Richard, F. Rob, E. Rossomme, T. Scheele, M. Scheurer, M. Schneider, N. Sergueev, S. M. Sharada, W. Skomorowski, D. W. Small, C. J. Stein, Y.-C. Su, E. J. Sundstrom, Z. Tao, J. Thirman, G. J. Tornai, T. Tsuchimochi, N. M. Tubman, S. P. Veccham, O. Vydrov, J. Wenzel, J. Witte, A. Yamada, K. Yao, S. Yeganeh, S. R. Yost, A. Zech, I. Y. Zhang, X. Zhang, Y. Zhang, D. Zuev, A. Aspuru-Guzik, A. T. Bell, N. A. Besley, K. B. Bravaya, B. R. Brooks, D. Casanova, J.-D. Chai, S. Coriani, C. J. Cramer, G. Cserey, A. E. DePrince, R. A. DiStasio, A. Dreuw, B. D. Dunietz, T. R. Furlani, W. A. Goddard, S. Hammes-Schiffer, T. Head-Gordon, W. J. Hehre, C.-P. Hsu, T.-C. Jagau, Y. Jung, A. Klamt, J. Kong, D. S. Lambrecht, W. Liang, N. J. Mayhall, C. W. McCurdy, J. B. Neaton, C. Ochsenfeld, J. A. Parkhill, R. Peverati, V. A. Rassolov, Y. Shao, L. V. Slipchenko, T. Stauch, R. P. Steele, J. E. Subotnik, A. J. W. Thom, A. Tkatchenko, D. G. Truhlar, T. Van Voorhis, T. A. Wesolowski,

K. B. Whaley, H. L. Woodcock, P. M. Zimmerman, S. Faraji, P. M. W. Gill, M. Head-Gordon, J. M. Herbert and A. I. Krylov, *J. Chem. Phys.*, 2021, **155**, 084801.
14) J.-D. Chai and M. Head-Gordon, *Phys. Chem. Chem. Phys.*, 2008, **10**, 6615.
15) J.-D. Chai and M. Head-Gordon, *The Journal of Chemical Physics*, 2008, **128**, 084106.
16) S. Kozuch and S. Shaik, *Acc. Chem. Res.*, 2011, **44**, 101–110.